

# Theory of Charmless Inclusive $B$ Decays and the Extraction of $V_{ub}$

BJÖRN O. LANGE<sup>a</sup>, MATTHIAS NEUBERT<sup>b</sup>, AND GIL PAZ<sup>b</sup>

<sup>a</sup> *Center for Theoretical Physics  
Massachusetts Institute of Technology  
Cambridge, MA 02139, U.S.A.*

<sup>b</sup> *Institute for High-Energy Phenomenology  
Newman Laboratory for Elementary-Particle Physics, Cornell University  
Ithaca, NY 14853, U.S.A.*

## Abstract

We present “state-of-the-art” theoretical expressions for the triple differential  $\bar{B} \rightarrow X_u l^- \bar{\nu}$  decay rate and for the  $\bar{B} \rightarrow X_s \gamma$  photon spectrum, which incorporate all known contributions and smoothly interpolate between the “shape-function region” of large hadronic energy and small invariant mass, and the “OPE region” in which all hadronic kinematical variables scale with  $M_B$ . The differential rates are given in a form which has no explicit reference to the mass of the  $b$  quark, avoiding the associated uncertainties. Dependence on  $m_b$  enters indirectly through the properties of the leading shape function, which can be determined by fitting the  $\bar{B} \rightarrow X_s \gamma$  photon spectrum. This eliminates the dominant theoretical uncertainties from predictions for  $\bar{B} \rightarrow X_u l^- \bar{\nu}$  decay distributions, allowing for a precise determination of  $|V_{ub}|$ . In the shape-function region, short-distance and long-distance contributions are factorized at next-to-leading order in renormalization-group improved perturbation theory. Higher-order power corrections include effects from subleading shape functions where they are known. When integrated over sufficiently large portions in phase space, our results reduce to standard OPE expressions up to yet unknown  $O(\alpha_s^2)$  terms. Predictions are presented for partial  $\bar{B} \rightarrow X_u l^- \bar{\nu}$  decay rates with various experimental cuts. An elaborate error analysis is performed that contains all significant theoretical uncertainties, including weak annihilation effects. We suggest that the latter can be eliminated by imposing a cut on high lepton invariant mass.

# 1 Introduction

A major effort of the  $B$ -physics community is underway to map out the apex of the unitarity triangle, which provides a graphical representation of the effect of CP violation in the quark flavor sector of the Standard Model. One of the biggest successes of this endeavor was the precise determination of the angle  $\beta$ , which has been measured with high accuracy from the time-dependent CP asymmetry in the  $B \rightarrow J/\psi K_S$  decay channel [1, 2]. The length of the side opposite the angle  $\beta$  is proportional to  $|V_{ub}|$ . A high-precision determination of this quantity would enable us to test the validity of the Standard Model and search for possible deviations from its predictions.

Good theoretical knowledge of strong-interaction effects in weak decays of  $B$  meson is crucial for a reliable exploration of the flavor sector of the Standard Model. In particular, the determination of the Cabibbo-Kobayashi-Maskawa (CKM) matrix elements  $|V_{cb}|$  and  $|V_{ub}|$  relies on an accurate description of bound-state effects in semileptonic decays. At present, the most precise calculations are available for inclusive semileptonic decays  $\bar{B} \rightarrow X l^- \bar{\nu}$ .

The theoretical tools for the calculation of inclusive  $B$  decays are QCD factorization on the one hand [3, 4, 5, 6, 7, 8, 9, 10, 11], and local operator product expansions (OPE) on the other [12, 13]. Both approaches perform a systematic separation of long-distance hadronic quantities from short-distance perturbative ones, while organizing the calculation in inverse powers of the heavy  $b$ -quark mass  $m_b$ . The OPE is an appropriate tool for the calculation of total inclusive rates (for example in  $\bar{B} \rightarrow X_c l^- \bar{\nu}$  decays) or for partial rates integrated over sufficiently large regions in phase space, where all components of the final-state hadronic momentum  $P_X^\mu$  are large compared with  $\Lambda_{\text{QCD}}$ . QCD factorization, on the other hand, is better suited for the calculation of partial rates and spectra near kinematical boundaries, where typically some components of  $P_X^\mu$  are large, while the invariant hadronic mass  $M_X = \sqrt{P_X^2}$  is small. For example, any  $\bar{B} \rightarrow X_u l^- \bar{\nu}$  event can be described with three independent kinematical variables, a useful choice of which is [9, 14]

$$P_l = M_B - 2E_l, \quad P_- = E_X + |\vec{P}_X|, \quad P_+ = E_X - |\vec{P}_X|. \quad (1)$$

Here  $P_\pm$  are the light-cone components of the hadronic final-state momentum along the jet direction,  $E_l$  is the charged-lepton energy,  $E_X$  is the jet energy, and  $\vec{P}_X$  is the jet momentum, all measured in the  $B$ -meson rest frame. In terms of these variables, the phase space is such that

$$\frac{M_\pi^2}{P_-} \leq P_+ \leq P_l \leq P_- \leq M_B, \quad (2)$$

with  $M_\pi$  being the mass of the lightest possible hadronic final state. The product  $P_+ P_- = M_X^2$  is the hadronic invariant mass squared. In order to avoid large backgrounds from  $b \rightarrow c$  transitions, all measurements of  $|V_{ub}|$  are in one way or another restricted to the region of phase space where  $P_+ P_- < M_D^2$ . If the quantity  $P_-$  is allowed to reach its maximum value near  $M_B$ , it follows that  $P_+$  is restricted to a region of order  $M_D^2/M_B$ , which is numerically comparable to  $\Lambda_{\text{QCD}}$ . This means that there are three parametrically different energy scales in the problem: the mass  $M_B$  of the initial state, the mass of the final hadronic state  $\sim \sqrt{M_B \Lambda_{\text{QCD}}}$ , and the low scale  $\Lambda_{\text{QCD}}$  at which perturbation theory breaks down and hadronic physics must be

parameterized in terms of non-perturbative matrix elements. QCD factorization disentangles the effects from these scales, so that the perturbative contributions can be expanded in powers of  $\alpha_s(\mu_h)$  with  $\mu_h \sim m_b$  (giving rise to “hard functions”) and  $\alpha_s(\mu_i)$  with  $\mu_i \sim \sqrt{m_b \Lambda_{\text{QCD}}}$  (giving rise to “jet functions”).

It is important to note that the heavy-quark expansions valid in these two kinematical regions are not identical, because the power counting rules differ in the two regimes. Also the nature of the non-perturbative inputs is different. In the OPE region, non-perturbative physics is encoded in a few hadronic parameters, and the heavy-quark expansion is the usual Wilsonian expansion in local operators. In the endpoint (or shape-function) region, the presence of multiple scales complicates the power counting, and the interplay between soft and collinear modes gives rise to large non-localities. As a result, non-perturbative physics is described by hadronic structure functions (called “shape functions”), and the heavy-quark expansion is an expansion in non-local string operators defined on the light-cone. The connections between the two regimes is that *moments* of the shape functions can be expressed in terms of local operators.

The goal of the present work is to develop a formalism that smoothly interpolates between the two kinematical regimes (see [15] for a related discussion, which is however restricted to the tree approximation). This is essential for building an event generator for inclusive  $\bar{B} \rightarrow X_u l^- \bar{\nu}$  and  $\bar{B} \rightarrow X_s \gamma$  decays, which can be used to study differential decay rates and partial decay rates in different kinematical domains. In the shape-function region, our approach relies on exact QCD factorization theorems, which exist in every order of power counting. They allow us to systematically disentangle short- and long-distance physics and, in the process, resum parametrically large logarithms order by order in perturbation theory. This factorization can be done with high accuracy for the terms of leading power in  $1/m_b$ , and with somewhat less sophistication for the first-order power corrections. For the second-order power corrections, we only include contributions that do not vanish when integrated over all phase space. This is a safe approximation; the effects of the remaining  $1/m_b^2$  terms can to a large extent be absorbed by a redefinition of the subleading shape functions arising at order  $1/m_b$ .

Our formalism is “optimized” for the shape-function region in the sense that sophisticated theoretical technology is applied in this regime. However, when our expressions for the differential decay rates are integrated over sufficiently wide domains, they automatically reduce to the simpler results that can be derived using the OPE approach, up to yet unknown terms of  $O(\alpha_s^2)$ . The moment relations for the shape functions are crucial in this regard. Note that local  $1/m_b^2$  corrections in the OPE receive contributions from terms of leading power ( $1/m_b^0$ ), subleading power ( $1/m_b$ ), and sub-subleading power ( $1/m_b^2$ ) in the shape-function region, so the transition is highly non-trivial. In implementing the program outlined here, we include all presently known information on the triple differential  $\bar{B} \rightarrow X_u l^- \bar{\nu}$  decay rate and on the differential  $\bar{B} \rightarrow X_s \gamma$  decay rate in a single, unified framework. We neglect, for simplicity, hadronic power corrections of order  $1/m_b^3$  and higher, which are known to have a negligible effect on the observables considered here. The only possible exception is contributions from “weak annihilation”, which are estimated as part of our error analysis. We also ignore the existing results on  $O(\beta_0 \alpha_s^2)$  radiative corrections, because they are only known for some single differential distributions, but neither for any double or triple differential  $\bar{B} \rightarrow X_u l^- \bar{\nu}$  spectra, nor for the  $\bar{B} \rightarrow X_s \gamma$  photon spectrum. While these corrections are sometimes found to be

large when naive perturbation theory in  $\alpha_s(m_b)$  is used, their effects are expected to be small in our scheme, which is based on a complete scale separation using QCD factorization. We see no reason why the  $\beta_0\alpha_s^2$  terms should be enhanced compared with other, unknown corrections of  $O(\alpha_s^2)$ .

A technical complication in realizing the approach described here has to do with the treatment of phase-space factors. The heavy-quark expansion of the hadronic tensor for  $\bar{B} \rightarrow X_u l^- \bar{\nu}$  decay gives rise to expressions that are singular at certain points in phase space. One way to avoid these singularities is to also expand phase-space factors order by order in  $1/m_b$  (see, e.g., the treatment in [16]). However, since this expansion depends on the kinematical cuts of any given analysis, it cannot be implemented in a straightforward way in an event generator. An alternative is to reorganize the heavy-quark expansion in such a way that the expansion parameter is related to *hadronic* (as opposed to *partonic*) kinematical variables, in which case kinematical singularities are always canceled by exact phase-space factors. Following this strategy, we obtain expressions for decay distributions and partial decay rates which are free of explicit reference to partonic quantities such as the  $b$ -quark mass. A dependence on  $m_b$  enters only implicitly via the first moment of the leading-order shape function denoted by  $\hat{S}(\hat{\omega})$ . The philosophy of our approach is that this function<sup>1</sup> is extracted experimentally from a fit to the  $\bar{B} \rightarrow X_s \gamma$  photon spectrum, which has been measured with increasing precision in the region where  $P_+ = M_B - 2E_\gamma \sim \Lambda_{\text{QCD}}$ . This is analogous to the extraction of parton distribution functions from deep inelastic scattering. The photon spectrum is experimentally accessible to energies as low as 1.8 GeV, which corresponds to a sampling of the shape function for values of  $\hat{\omega}$  up to around 1.7 GeV. Once the shape function has been extracted over this range, we can use it to obtain predictions for arbitrary partial  $\bar{B} \rightarrow X_u l^- \bar{\nu}$  decay rates with cuts. In doing so, the residual hadronic uncertainties in the extraction of  $|V_{ub}|$  only enter at the level of power corrections.

We emphasize that the program outlined above is equivalent to an approach put forward in [4] and later refined in [17, 18, 19], in which  $|V_{ub}|$  is extracted with the help of shape-function independent relations between weighted integrals over differential decay distributions in  $\bar{B} \rightarrow X_s \gamma$  and  $\bar{B} \rightarrow X_u l^- \bar{\nu}$ . The experimental error in the results for these weighted integrals corresponds, in our approach, to the error in the prediction of  $\bar{B} \rightarrow X_u l^- \bar{\nu}$  partial rates resulting from the experimental uncertainty in the extraction of the shape function from the  $\bar{B} \rightarrow X_s \gamma$  photon spectrum. While the shape-function independent relations are very elegant, it is more convenient for the construction of a generator to have a formulation where the shape function is used as an input. In this way, it is possible to impose arbitrary cuts on kinematical variables without having to recompute the weight functions in each case.

The paper is structured as follows: In Section 2 we collect the relevant formulae for the calculation of the  $\bar{B} \rightarrow X_s \gamma$  photon spectrum. These expressions can be used to extract the leading non-perturbative structure function from experiment. An analogous presentation for the triple differential decay rate in  $\bar{B} \rightarrow X_u l^- \bar{\nu}$  decays is given in Section 3. In order to perform a numerical analysis one needs to rely on parameterizations of the shape functions. A

---

<sup>1</sup>More precisely, we define a new shape function  $\hat{S}(\hat{\omega})$  by the combination of leading and subleading shape functions contributing to  $\bar{B} \rightarrow X_s \gamma$  decay, and we will use the same function to make predictions for  $\bar{B} \rightarrow X_u l^- \bar{\nu}$  decay distributions.

collection of several useful functional forms is given in Section 4. In Section 5 we present a full error analysis of partial  $\bar{B} \rightarrow X_u l^- \bar{\nu}$  decay rates for a variety of experimental cuts. We also explore the sensitivity of the results to the  $b$ -quark mass and to the functional forms adopted for the shape functions. Section 6 contains our conclusions.

## 2 Inclusive radiative decays

The decay process  $\bar{B} \rightarrow X_s \gamma$ , while more complex in its short-distance physics, is considerably simpler in its kinematics than the semileptonic process  $\bar{B} \rightarrow X_u l^- \bar{\nu}$ . Since the radiated photon is on-shell, the hadronic variables  $P_{\pm}$  that describe the momentum of the  $X_s$  system are trivially related to the photon energy  $E_{\gamma}$  by  $P_+ = M_B - 2E_{\gamma}$  and  $P_- = M_B$ . In the crudest approximation, namely at tree level and leading power, the photon-energy spectrum is directly proportional to the leading shape function,  $d\Gamma_s/dE_{\gamma} \propto \hat{S}(P_+)$ . In this section we collect all relevant formulae needed to compute the  $\bar{B} \rightarrow X_s \gamma$  photon spectrum (or, equivalently, the invariant hadronic mass distribution).

The differential decay rate can be written as

$$\frac{d\Gamma_s}{dE_{\gamma}} = \frac{G_F^2 \alpha}{2\pi^4} E_{\gamma}^3 |V_{tb} V_{ts}^*|^2 \bar{m}_b^2(\mu_h) [C_{7\gamma}^{\text{eff}}(\mu_h)]^2 U(\mu_h, \mu_i) \mathcal{F}_{\gamma}(P_+), \quad (3)$$

where the structure function  $\mathcal{F}_{\gamma}$  depends on the photon energy via  $P_+ = M_B - 2E_{\gamma}$ . The prefactor contains the electromagnetic fine-structure constant  $\alpha$  normalized at  $q^2 = 0$ , two powers of the running  $b$ -quark mass (defined in the  $\overline{\text{MS}}$  scheme) originating from the electromagnetic dipole operator  $Q_{7\gamma}$  in the effective weak Hamiltonian, and the square of the corresponding Wilson coefficient  $C_{7\gamma}^{\text{eff}}$ , which is needed at next-to-leading order in renormalization-group improved perturbation theory [20]. Renormalization-group running from the hard scale  $\mu_h \sim m_b$  to the intermediate scale  $\mu_i \sim \sqrt{m_b \Lambda_{\text{QCD}}}$  gives rise to the Sudakov factor  $U(\mu_h, \mu_i)$ , whose explicit form is discussed in Appendix A.2. We keep  $U$  and  $(C_{7\gamma}^{\text{eff}})^2$  outside of the structure function  $\mathcal{F}_{\gamma}$ ; it is understood that when combining the various terms in (3) all perturbative quantities should be expanded for consistency to the required order in  $\alpha_s$ .

### 2.1 Leading-power factorization formula

At leading order in  $1/m_b$  the structure function  $\mathcal{F}_{\gamma}$  factorizes as [11]

$$\mathcal{F}_{\gamma}^{(0)}(P_+) = |H_s(\mu_h)|^2 \int_0^{P_+} d\hat{\omega} m_b J(m_b(P_+ - \hat{\omega}), \mu_i) \hat{S}(\hat{\omega}, \mu_i). \quad (4)$$

At this order a single non-perturbative parton distribution function arises, called the leading shape function [4] and denoted by  $\hat{S}(\hat{\omega}, \mu_i)$ . Our notation is adopted from [9, 16]: hatted shape functions are defined on the interval  $\hat{\omega} \in [0, M_B]$ . The function  $\hat{S}$  is defined in terms of a non-local matrix element in heavy-quark effective theory (HQET). Renormalization-group running between the intermediate scale and a low hadronic scale is avoided when using the shape functions renormalized at the intermediate scale  $\mu_i$ . Evolution effects below this scale

are universal (i.e., process independent) and so can be absorbed into the renormalized shape function. Short-distance contributions from scales above  $\mu_h \sim m_b$  are included in the hard function  $H_s$ , which in practice is obtained by matching the effective weak Hamiltonian onto a current operator in soft-collinear effective theory (SCET). At next-to-leading order in perturbation theory, the result reads

$$\begin{aligned}
H_s(\mu_h) = & 1 + \frac{C_F \alpha_s(\mu_h)}{4\pi} \left( -2 \ln^2 \frac{m_b}{\mu_h} + 7 \ln \frac{m_b}{\mu_h} - 6 - \frac{\pi^2}{12} \right) + \varepsilon_{\text{ew}} \\
& + \frac{C_{8g}^{\text{eff}}(\mu_h)}{C_{7\gamma}^{\text{eff}}(\mu_h)} \frac{C_F \alpha_s(\mu_h)}{4\pi} \left( -\frac{8}{3} \ln \frac{m_b}{\mu_h} + \frac{11}{3} - \frac{2\pi^2}{9} + \frac{2\pi i}{3} \right) \\
& + \frac{C_1(\mu_h)}{C_{7\gamma}^{\text{eff}}(\mu_h)} \frac{C_F \alpha_s(\mu_h)}{4\pi} \left( \frac{104}{27} \ln \frac{m_b}{\mu_h} + g(z) - \frac{V_{ub} V_{us}^*}{V_{tb} V_{ts}^*} [g(0) - g(z)] \right) + \varepsilon_{\text{peng}}, \quad (5)
\end{aligned}$$

where the variable  $z = (m_c/m_b)^2$  denotes the ratio of quark masses relevant to charm-loop penguin diagrams, and the ‘‘penguin function’’  $g(z)$  can be approximated by the first few terms of its Taylor expansion,

$$\begin{aligned}
g(z) = & -\frac{833}{162} - \frac{20\pi i}{27} + \frac{8\pi^2}{9} z^{3/2} \\
& + \frac{2z}{9} [48 - 5\pi^2 - 36\zeta_3 + (30\pi - 2\pi^3)i + (36 - 9\pi^2 + 6\pi i) \ln z + (3 + 6\pi i) \ln^2 z + \ln^3 z] \\
& + \frac{2z^2}{9} [18 + 2\pi^2 - 2\pi^3 i + (12 - 6\pi^2) \ln z + 6\pi i \ln^2 z + \ln^3 z] \\
& + \frac{z^3}{27} [-9 - 14\pi^2 + 112\pi i + (182 - 48\pi i) \ln z - 126 \ln^2 z] + \dots \quad (6)
\end{aligned}$$

The Wilson coefficients  $C_1$  and  $C_{8g}^{\text{eff}}$  in (5) multiply the current-current operators  $Q_1^{u,c}$  and the chromomagnetic dipole operator  $Q_{8g}$  in the effective weak Hamiltonian. The quantities  $\varepsilon_{\text{ew}} \approx -1.5\%$  and  $\varepsilon_{\text{peng}} \approx -0.6\%$  account for small electroweak corrections and the effects of penguin contractions of operators other than  $Q_1^{u,c}$ , respectively. The differential decay rate (3) is formally independent of the matching scales  $\mu_h$  and  $\mu_i$ . The dependence on the hard scale in the Sudakov factor is canceled by the hard function, and the  $\mu_i$  dependence compensates the scale dependence of the convolution integral  $J(\mu_i) \otimes \hat{S}(\mu_i)$ .

Finally let us discuss the jet function  $J$ , which appears as the hard-scattering kernel in the convolution integral in (4). It can be written in terms of distributions that act on the shape function  $\hat{S}$ . At one-loop level, the jet function is given by [8, 9]

$$J(p^2, \mu) = \delta(p^2) \left[ 1 + \frac{C_F \alpha_s(\mu)}{4\pi} (7 - \pi^2) \right] + \frac{C_F \alpha_s(\mu)}{4\pi} \left[ \frac{1}{p^2} \left( 4 \ln \frac{p^2}{\mu^2} - 3 \right) \right]_*^{[\mu^2]}, \quad (7)$$

where the star distributions have the following effect on a function  $f$  when integrated over a

domain  $Q^2$  [21]:

$$\int_{\leq 0}^{Q^2} dp^2 \left[ \frac{1}{p^2} \right]_*^{[\mu^2]} f(p^2) = \int_0^{Q^2} dp^2 \frac{f(p^2) - f(0)}{p^2} + f(0) \ln \frac{Q^2}{\mu^2},$$

$$\int_{\leq 0}^{Q^2} dp^2 \left[ \frac{1}{p^2} \ln \frac{p^2}{\mu^2} \right]_*^{[\mu^2]} f(p^2) = \int_0^{Q^2} dp^2 \frac{f(p^2) - f(0)}{p^2} \ln \frac{p^2}{\mu^2} + \frac{f(0)}{2} \ln^2 \frac{Q^2}{\mu^2}. \quad (8)$$

## 2.2 Kinematical power corrections

There exists a class of power corrections to (4) that do not involve new hadronic quantities. Instead, the power suppression results from the restriction of certain variables ( $P_+$  in the present case) to a region where they are kinematically suppressed (here  $P_+ \ll M_B$ ). The corresponding terms are known in fixed-order perturbation theory, without scale separation and renormalization-group resummation [22, 23] (see also [24]). To perform a complete RG analysis of even the first-order terms in  $1/m_b$  is beyond the scope of the present work. Since, as we will see later, power corrections only account for small corrections to the decay rates, an approximate treatment will suffice. To motivate it, we note the following two facts [11]: First, while the anomalous dimensions of the relevant subleading SCET and HQET operators are only known for a few cases [25], the leading Sudakov double logarithms are the same as for the terms of leading power, because they have a geometric origin in terms of Wilson lines [26]. The leading Sudakov double logarithms are therefore the same as those resummed into the function  $U$  in (3). Secondly, the kinematical power corrections in  $\bar{B} \rightarrow X_s \gamma$  decay are associated with gluon emission into the hadronic final state  $X_s$ . Because of the kinematical restriction to low-mass final states, i.e.  $M_X^2 \sim M_B \Lambda_{\text{QCD}}$ , we associate a coupling  $\alpha_s(\bar{\mu})$  with these terms, where typically  $\bar{\mu} \sim \mu_i$ . Strictly speaking, however, the scale ambiguity associated with the choice of  $\bar{\mu}$  could only be resolved by computing the relevant anomalous dimensions.

Within this approximation, the kinematical power corrections to the structure function  $\mathcal{F}_\gamma$  can be extracted from [11, 24]. We find it convenient to express the result in terms of the variable

$$x = \frac{P_+ - \hat{\omega}}{M_B - P_+}, \quad (9)$$

which in the shape-function region scales like  $\Lambda_{\text{QCD}}/m_b$ . We obtain

$$\mathcal{F}_\gamma^{\text{kin}}(P_+) = \frac{1}{M_B - P_+} \frac{C_F \alpha_s(\bar{\mu})}{4\pi} \sum_{\substack{i,j=1,7,8 \\ i \leq j}} \frac{C_i(\mu_h) C_j(\mu_h)}{C_{7\gamma}^{\text{eff}}(\mu_h)^2} \int_0^{P_+} d\hat{\omega} \hat{S}(\hat{\omega}, \mu_i) h_{ij}(x)$$

$$- \frac{\lambda_2}{9m_c^2} \frac{C_1(\mu_h)}{C_{7\gamma}^{\text{eff}}(\mu_h)} \hat{S}(P_+, \mu_i). \quad (10)$$

The coefficient functions  $h_{ij}(x)$  are

$$\begin{aligned}
h_{77}(x) &= -3(5 + 2x) + 2(8 + 9x + 3x^2) \ln \left( 1 + \frac{1}{x} \right), \\
h_{88}(x) &= \frac{2}{9} (1 + 3x + 4x^2 + 2x^3) \left[ 2 \ln \frac{m_b}{m_s} - \ln \left( 1 + \frac{1}{x} \right) \right] - \frac{1}{9} (3 + 9x + 16x^2 + 8x^3), \\
h_{78}(x) &= \frac{2}{3} (5 + 8x + 4x^2) - \frac{8}{3} x(1 + x)^2 \ln \left( 1 + \frac{1}{x} \right), \\
h_{11}(x) &= \frac{16}{9} \int_0^1 du (1 + x - u) \left| \frac{z(1+x)}{u} G \left( \frac{u}{z(1+x)} \right) + \frac{1}{2} \right|^2, \\
h_{17}(x) &= -3h_{18}(x) = -\frac{8}{3} \int_0^1 du u \operatorname{Re} \left[ \frac{z(1+x)}{u} G \left( \frac{u}{z(1+x)} \right) + \frac{1}{2} \right], \tag{11}
\end{aligned}$$

where as before  $z = (m_c/m_b)^2$ , and

$$G(t) = \begin{cases} -2 \arctan^2 \sqrt{t/(4-t)} & ; t < 4, \\ 2 \left( \ln \left[ (\sqrt{t} + \sqrt{t-4})/2 \right] - \frac{i\pi}{2} \right)^2 & ; t \geq 4. \end{cases} \tag{12}$$

In the shape-function region the expressions for  $h_{ij}(x)$  could, if desired, be expanded in a power series in  $x = O(\Lambda_{\text{QCD}}/m_b)$ , and this would generate a series of power-suppressed terms  $\mathcal{F}_\gamma^{\text{kin}(n)}(P_+)$  with  $n \geq 1$ , where the superscript “n” indicates the order in the  $1/m_b$  expansion. Note that this expansion would contain single logarithms  $\ln x \sim \ln(\Lambda_{\text{QCD}}/m_b)$ . These are precisely the logarithms that would be resummed in a more proper treatment using effective field-theory methods.

Outside the shape-function region the variable  $x$  can take on arbitrarily large positive values, and  $\mathcal{F}_\gamma^{\text{kin}}(P_+)$  is no longer power suppressed. Note for  $P_+ \rightarrow M_B$  (corresponding to  $x \rightarrow \infty$  and  $E_\gamma \rightarrow 0$ ), most functions  $h_{ij}(x)$  grow like  $x^2$  or weaker, so that the spectrum tends to a constant. The only (well known) exception is  $h_{88}(x)$ , which grows like  $x^3$ , giving rise to a  $1/E_\gamma$  soft-photon singularity [23].

The main effect of the kinematical power corrections (10) to the photon spectrum is the appearance of a radiative tail extending into the region of smaller photon energies. These corrections therefore become more significant when the domain of integration over  $E_\gamma$  is increased.

### 2.3 Subleading shape-function contributions

At order  $1/m_b$  in power counting, different combinations of subleading shape functions enter the  $\bar{B} \rightarrow X_s \gamma$  and  $\bar{B} \rightarrow X_u l^- \bar{\nu}$  decay distributions [27, 28, 29, 30]. They provide the dominant “hadronic” power corrections, which must be combined with the “kinematic” power corrections discussed in the previous section. We include their effects using the results of recent calculations in [16, 31, 32]. Little is known about the subleading shape functions apart from

expressions for their first few moments. In particular, the norms of these functions vanish at tree level, while their first moments are determined by the HQET parameters  $\lambda_1$  and  $\lambda_2$ , which are defined via the forward  $B$ -meson matrix elements of the kinetic-energy and the chromo-magnetic operators, respectively [33].

For the case of  $\bar{B} \rightarrow X_s \gamma$  decay, subleading shape-function contributions are currently only known for the matrix elements of the dipole operator  $Q_{7\gamma}$ , and the corresponding hard and jet functions have been computed at tree level. Adopting the notations of [16], the relevant subleading shape functions are  $\hat{t}(\hat{\omega})$ ,  $\hat{u}(\hat{\omega})$ , and  $\hat{v}(\hat{\omega})$ . An additional function, called  $s_0$ , has been absorbed by a redefinition of the leading shape function, and it is included in our definition of  $\hat{S}(\hat{\omega})$ . Roughly speaking,  $\hat{u}(\hat{\omega})$  is the “light-cone generalization” of the local HQET kinetic-energy operator. The functions  $\hat{v}(\hat{\omega})$  and  $\hat{t}(\hat{\omega})$  are both generalizations of the local chromo-magnetic HQET operator, but  $\hat{t}(\hat{\omega})$  contains also a light-cone chromo-electric operator, which has no equivalent in the local OPE expansion. (Such a contribution arises since in the SCET expansion we have two external 4-vectors,  $n$  and  $v$ , while in the HQET expansion we have only  $v$ .) The contribution of subleading shape functions to the  $\bar{B} \rightarrow X_s \gamma$  photon spectrum is

$$\mathcal{F}_\gamma^{\text{hadr}(1)}(P_+) = \frac{1}{M_B - P_+} \left[ -(\bar{\Lambda} - P_+) \hat{S}(P_+) - \hat{t}(P_+) + \hat{u}(P_+) - \hat{v}(P_+) \right]. \quad (13)$$

Compared to [16], we have replaced  $1/m_b$  with  $1/(M_B - P_+)$  in the prefactor, which is legitimate at this order. (The form of the shape functions restricts  $P_+$  to be of order  $\Lambda_{\text{QCD}}$ .) The appearance of the HQET parameter  $\bar{\Lambda} = (M_B - m_b)_{m_b \rightarrow \infty}$  is peculiar to the subleading shape-function contributions. This quantity is defined via the first moment of the leading-order shape function.

The formula given above can be modified to suit the purpose of extracting the shape function from the photon spectrum better. To this end, we absorb a linear combination of the subleading shape functions into a redefinition of the leading shape function, in such a way that the moment relations for the leading structure function remain unchanged to the order we are working. This is accomplished by defining

$$\hat{\mathcal{S}}(\hat{\omega}) \equiv \hat{S}(\hat{\omega}) + \frac{2(\bar{\Lambda} - \hat{\omega}) \hat{S}(\hat{\omega}) - \hat{t}(\hat{\omega}) + \hat{u}(\hat{\omega}) - \hat{v}(\hat{\omega})}{m_b}. \quad (14)$$

When using  $\hat{\mathcal{S}}$  instead of  $\hat{S}$  in the leading-power formula (4), the subleading shape-function contribution becomes

$$\mathcal{F}_\gamma^{\text{hadr}(1)}(P_+) = -\frac{3(\bar{\Lambda} - P_+)}{M_B - P_+} \hat{\mathcal{S}}(P_+). \quad (15)$$

The hatted shape functions used in the present work are related to the original definitions in [16] by

$$\hat{S}(\hat{\omega}) = S(\bar{\Lambda} - \hat{\omega}) + \frac{s_0(\bar{\Lambda} - \hat{\omega})}{m_b}, \quad \hat{t}(\hat{\omega}) = t(\bar{\Lambda} - \hat{\omega}), \quad \text{etc.}, \quad (16)$$

where the unhatted functions have support on the interval between  $-\infty$  and  $\bar{\Lambda}$ . It is convenient to rewrite  $\bar{\Lambda} - \hat{\omega} = \omega + \Delta\omega$ , where

$$\Delta\omega \equiv \bar{\Lambda} - (M_B - m_b) = \frac{\lambda_1 + 3\lambda_2}{2m_b} + \dots \quad (17)$$

accounts for the mismatch between the HQET parameter  $\bar{\Lambda}$  and the difference  $(M_B - m_b)$  due to power-suppressed terms in the  $1/m_b$  expansion [34]. It follows that the variable  $\omega = (M_B - m_b) - \hat{\omega}$  runs from  $-\infty$  to  $(M_B - m_b)$ . The moment relations for the leading and subleading shape functions derived in [4] and [16, 27] can be summarized as

$$\begin{aligned}
\hat{S}(\hat{\omega}) &\equiv S(\omega + \Delta\omega) + \frac{s_0(\omega + \Delta\omega)}{m_b} = \delta(\omega) - \frac{\lambda_1}{6} \delta''(\omega) + \frac{\lambda_1 + 3\lambda_2}{2m_b} \delta'(\omega) + \dots, \\
\hat{t}(\hat{\omega}) &\equiv t(\omega + \Delta\omega) = \lambda_2 \delta'(\omega) + \dots, \\
\hat{u}(\hat{\omega}) &\equiv u(\omega + \Delta\omega) = -\frac{2\lambda_1}{3} \delta'(\omega) + \dots, \\
\hat{v}(\hat{\omega}) &\equiv v(\omega + \Delta\omega) = -\lambda_2 \delta'(\omega) + \dots.
\end{aligned} \tag{18}$$

The function  $\hat{\mathcal{S}}$  has the same moment expansion as  $\hat{S}$ . The hadronic parameter  $\lambda_2$  determines the leading contribution to the hyperfine splitting between the masses of  $B$  and  $B^*$  mesons through  $m_{B^*}^2 - m_B^2 = 4\lambda_2 + O(1/m_b)$  [33], from which it follows that  $\lambda_2 \approx 0.12 \text{ GeV}^2$ . The value of the parameter  $\lambda_1$  is more uncertain. In much the same way as the  $b$ -quark pole mass, it is affected by infrared renormalon ambiguities [35, 36]. It is therefore better to eliminate  $\lambda_1$  in favor of some observable, for which we will choose the width of the leading shape function.

## 2.4 Residual hadronic power corrections

At order  $1/m_b^2$  a new set of sub-subleading shape functions enter, which so far have not been classified completely in the literature. Since the functional form of even the subleading shape functions is rather uncertain, there is no need to worry too much about the precise form of sub-subleading shape functions. Most of their effects can be absorbed into the subleading functions. An exception, however, are terms that survive when the sub-subleading shape functions are integrated over a wide domain. Whereas the norms of all subleading ( $\sim 1/m_b$ ) shape functions vanish, the norms of the sub-subleading shape functions ( $\sim 1/m_b^2$ ) are in general non-zero and given in terms of the heavy-quark parameters  $\lambda_1$  and  $\lambda_2$ . (At tree level, the class of functions with non-zero norm has been studied in [15].) Our strategy in the present work will be as follows: We start from the well-known expressions for the (tree-level) second-order power corrections to the  $\bar{B} \rightarrow X_s \gamma$  photon spectrum [37] (and similarly for the triple-differential  $\bar{B} \rightarrow X_u l^- \bar{\nu}$  decay distribution [12, 13], see Section 3.4). They are of the form  $\lambda_i/m_b^2$  times one of the singular distributions  $\delta(p^2)$ ,  $\delta'(p^2)$ , or  $\delta''(p^2)$ , where  $p^2 = (m_b v - q)^2$  is the invariant partonic mass squared of the final-state jet. As mentioned earlier, the power counting in the shape-function region is different from the one used in OPE calculations, and indeed a good portion of these OPE  $1/m_b^2$  terms is already accounted for by the contributions proportional to the leading and sub-leading shape functions in (4) and (13), respectively. We identify the corresponding terms using the moment relations for the shape functions in (18). In particular, this accounts for all terms at order  $1/m_b^2$  in the OPE which contain derivatives

of  $\delta(p^2)$ . We account for the remaining terms of the form  $(\lambda_i/m_b^2)\delta(p^2)$  by replacing

$$\begin{aligned}\delta(p^2) &= \delta(p_+p_-) = \frac{1}{p_- - p_+} \int d\omega \delta(p_+ + \omega) \delta(\omega) \\ &\rightarrow \frac{1}{P_- - P_+} \int d\hat{\omega} \delta(P_+ - \hat{\omega}) \hat{S}(\hat{\omega}) = \frac{\hat{S}(P_+)}{P_- - P_+}.\end{aligned}\quad (19)$$

Here  $p_{\pm}$  are the light-cone projections of the partonic momentum  $p^{\mu}$ , which are related to the hadronic quantities  $P_{\pm}$  by  $P_{\pm} = p_{\pm} + (M_B - m_b)$ . Similarly,  $\hat{\omega} = (M_B - m_b) - \omega$ .

The result of these manipulations is

$$\mathcal{G}_{\gamma}^{\text{had}(2)} = \frac{\lambda_1}{(M_B - P_+)^2} \hat{S}(P_+).\quad (20)$$

Together with (4) and (13), this accounts for all known first- and second-order power corrections to the  $\bar{B} \rightarrow X_s \gamma$  photon spectrum, both in the shape-function region and in the OPE region. The redefinition (14) of the leading shape function from  $\hat{S}$  to  $\hat{\mathcal{S}}$  leaves the form of the second-order power corrections unaffected.

In Section 5 we study the numerical impact of second-order power corrections on various  $\bar{B} \rightarrow X_u l^- \bar{\nu}$  partial rates and find their effects to be tiny. It is therefore a safe approximation to neglect hadronic power corrections of order  $1/m_b^3$  or higher. The only possible exception to this conclusion relates to so-called weak annihilation terms in  $\bar{B} \rightarrow X_u l^- \bar{\nu}$  decay, which will be included in our error analysis.

### 3 Inclusive semileptonic decays

All hadronic physics in  $\bar{B} \rightarrow X_u l^- \bar{\nu}$  decays is encoded in the hadronic tensor  $W^{\mu\nu}$ , which is defined via the discontinuity of the forward  $B$ -meson matrix element of a correlator of two flavor-changing weak currents  $J^{\mu} = \bar{u} \gamma^{\mu} (1 - \gamma_5) b$ . Explicitly it is

$$W^{\mu\nu} = \frac{1}{2M_B} \frac{1}{\pi} \text{Im} \langle \bar{B}(v) | i \int d^4x e^{iq \cdot x} \text{T} \{ J^{\dagger\mu}(0), J^{\nu}(x) \} | \bar{B}(v) \rangle,\quad (21)$$

where  $v$  is the  $B$ -meson velocity, and  $q$  the momentum carried by the lepton pair. The hadronic tensor decomposes into five structure functions  $W_i$ , which are the coefficients of the five possible Lorentz structures built out of two independent 4-vectors. Typical choices for these two vectors are  $q$  and  $v$ ,  $p$  and  $v$ , etc. Here, as above,  $p = m_b v - q$  is the momentum of the jet of light particles into which the  $b$  quark decays. In principle, all choices are equivalent, and it is solely a matter of convenience which basis one picks.

The triple differential decay rate can then be expressed in terms of kinematical prefactors and the functions  $W_i$ . It is a known fact that the total decay rate is proportional to five powers of the  $b$ -quark mass. Further sensitivity to  $m_b$  is picked up for partial decay rates by the kinematical cuts. For example, cutting on the leptonic invariant mass  $q^2 > q_0^2$  introduces roughly five additional powers, and the resulting partial decay rate is proportional to  $(m_b)^a$  with  $a \approx 10$  [38, 39]. This is the reason why theoretical predictions were typically made for

event fractions, so that at least the five powers of  $m_b$  in the total rate drop out. For practical purposes, however, this procedure presents no advantage as the value of the total decay rate cannot be measured. Furthermore, the  $m_b$  dependence of the total rate is clearly related to the  $m_b$  dependence of partial rates, and it is important to take this correlation into account when combining calculations of event fractions with those of the total decay rate. In Section 5, where we present theoretical predictions, we will thus focus directly on predictions of partial decay rates, not event fractions. The question at hand is how information about  $m_b$  enters the triple differential decay rate. Potentially there are two sources, the hadronic structure functions  $W_i$  and their kinematical prefactors. Whether or not  $m_b$  appears explicitly in the prefactors depends on the decomposition of  $W^{\mu\nu}$ , i.e. the choice of vectors used to form the five possible Lorentz structures.

A very useful set of 4-vectors turns out to be  $(v, n)$ , where  $n$  is a light-like vector in the direction of the jet of light particles. In SCET,  $n$  denotes the direction of the collinear particles in the jet, which is typically set to be along the  $z$ -axis. The normalization is chosen such that  $v \cdot n = 1$ , so that  $n^\mu = (1, 0, 0, 1)$  in the rest frame of the  $B$  meson. The conjugate direction to  $n$  is denoted by  $\bar{n}^\mu = (1, 0, 0, -1)$  and marks the direction of the photon in  $\bar{B} \rightarrow X_s \gamma$  decays, or the direction of the lepton pair in  $\bar{B} \rightarrow X_u l^- \bar{\nu}$  decays. We then decompose

$$W^{\mu\nu} = (n^\mu v^\nu + n^\nu v^\mu - g^{\mu\nu} - i\epsilon^{\mu\nu\alpha\beta} n_\alpha v_\beta) \tilde{W}_1 - g^{\mu\nu} \tilde{W}_2 + v^\mu v^\nu \tilde{W}_3 + (n^\mu v^\nu + n^\nu v^\mu) \tilde{W}_4 + n^\mu n^\nu \tilde{W}_5. \quad (22)$$

The structure functions  $\tilde{W}_i$  all have mass dimension  $-1$  in this basis. In terms of the  $\tilde{W}_i$  functions the triple differential decay rate reads

$$\frac{d^3\Gamma_u}{dP_+ dP_- dP_l} = \frac{G_F^2 |V_{ub}|^2}{16\pi^3} U_y(\mu_h, \mu_i) (M_B - P_+) \left[ (P_- - P_l)(M_B - P_- + P_l - P_+) \mathcal{F}_1 + (M_B - P_-)(P_- - P_+) \mathcal{F}_2 + (P_- - P_l)(P_l - P_+) \mathcal{F}_3 \right], \quad (23)$$

where we have collected the relevant combinations of  $\tilde{W}_i$  into the three functions

$$U_y(\mu_h, \mu_i) \mathcal{F}_1 = \tilde{W}_1, \quad U_y(\mu_h, \mu_i) \mathcal{F}_2 = \frac{\tilde{W}_2}{2}, \quad U_y(\mu_h, \mu_i) \mathcal{F}_3 = \left( \frac{y}{4} \tilde{W}_3 + \tilde{W}_4 + \frac{1}{y} \tilde{W}_5 \right), \quad (24)$$

and defined a new kinematical variable

$$y = \frac{P_- - P_+}{M_B - P_+}, \quad (25)$$

which can take values  $0 \leq y \leq 1$ . The leading Sudakov factor  $U_y(\mu_h, \mu_i)$  has been factored out in (23) for convenience, as we have done earlier in (3). The function  $U_y(\mu_h, \mu_i)$  differs from the corresponding function in  $\bar{B} \rightarrow X_s \gamma$  decay by a  $y$ -dependent factor,

$$U_y(\mu_h, \mu_i) = U(\mu_h, \mu_i) y^{-2a_\Gamma(\mu_h, \mu_i)}, \quad (26)$$

where the function  $a_\Gamma$  in the exponent is related to the cusp anomalous dimension and is given in Appendix A.2.

Eq. (23) for the triple differential rate is exact. Note that there is no reference to the  $b$ -quark mass at this point. The only dependence on  $m_b$  is through the structure functions  $\mathcal{F}_i(P_+, y)$  (via hard matching corrections and via the moment constraints on the shape function  $\hat{S}$ ), which are independent of the leptonic variable  $P_l$ . The fact that the total decay rate  $\Gamma_u$  is proportional to  $m_b^5$  is not in contradiction with (23). It is instructive to demonstrate how these five powers of  $m_b$  are recovered in our approach. At tree level and leading power the functions  $\mathcal{F}_2$  and  $\mathcal{F}_3$  vanish, while  $\mathcal{F}_1 = \hat{S}(P_+)$ . Integrating over the full range of  $P_l$  and  $P_-$  builds up five powers of  $(M_B - P_+)$ . For the purpose of illustration, let us rename the  $P_+$  variable to  $\hat{\omega}$  in the last integration, so that the total decay rate is given as

$$\begin{aligned} \Gamma_u &= \frac{G_F^2 |V_{ub}|^2}{192\pi^3} \int_0^{M_B} d\hat{\omega} (M_B - \hat{\omega})^5 \hat{S}(\hat{\omega}) = \frac{G_F^2 |V_{ub}|^2}{192\pi^3} \int_{-m_b}^{M_B - m_b} d\omega (m_b + \omega)^5 S(\omega) \\ &= \frac{G_F^2 |V_{ub}|^2}{192\pi^3} (m_b + \langle\omega\rangle)^5 \left[ 1 + O\left(\frac{1}{m_b^2}\right) \right]. \end{aligned} \quad (27)$$

At tree level, the first moment of the shape function  $S(\omega)$  vanishes. Beyond tree level this is no longer the case, and the average  $\langle\omega\rangle$  depends on the size of the integration domain. The above observation motivates the use of the shape-function scheme [9], in which the  $b$ -quark mass is defined as  $m_b^{\text{SF}} = m_b^{\text{pole}} + \langle\omega\rangle + O(1/m_b)$ . After this is done, (27) recovers the form of the conventional OPE result.

Eq. (23) and the above argument tell us that the differential rate is a priori rather insensitive to the  $b$ -quark mass in the endpoint region, where  $P_+$  (and therefore  $\langle\hat{\omega}\rangle$ ) is a small quantity. Only when the rates are integrated over a sufficiently wide domain, so that shape-function integrals can be approximated using a moment expansion, a dependence on  $m_b$  enters indirectly via the first moment of the leading-order shape functions. Likewise, a dependence on other HQET parameters such as  $\lambda_1$  enters via the sensitivity to higher moments.

In the remainder of this section we present the various contributions to the structure functions  $\mathcal{F}_i$ , following the same line of presentation as we did in the case of  $\bar{B} \rightarrow X_s \gamma$  decay in Section 2. As before, while the resulting expressions are “optimized” for the shape-function region, they can be used over the entire phase space and give the correct result for the total decay rate up to corrections of  $O(\alpha_s^2)$ . In the shape-function region, where  $P_+$  is a small quantity, one may organize  $\mathcal{F}_i$  as a series in inverse powers of  $1/(M_B - P_+)$ . No assumption about the variable  $y$  is made, which is treated as an  $O(1)$  quantity.<sup>2</sup> A preview of the results of our calculation is depicted in Figure 1, which shows an illustration of our prediction of the distribution of events in the plane  $(P_+, P_-)$ .

### 3.1 Leading-power factorization formula

The leading-power expressions for the hadronic structure functions  $W_i$  have been calculated in [9] at one-loop order in renormalization-group improved perturbation theory. At this level  $\mathcal{F}_2$  does not obtain a contribution, whereas  $\mathcal{F}_1$  and  $\mathcal{F}_3$  do. Symbolically, they take the factorized

---

<sup>2</sup>In the shape-function region, where  $P_+ \ll P_-$ , we have  $y \approx p_-/m_b$ , which is the variable used in the leading-power analysis in [9].

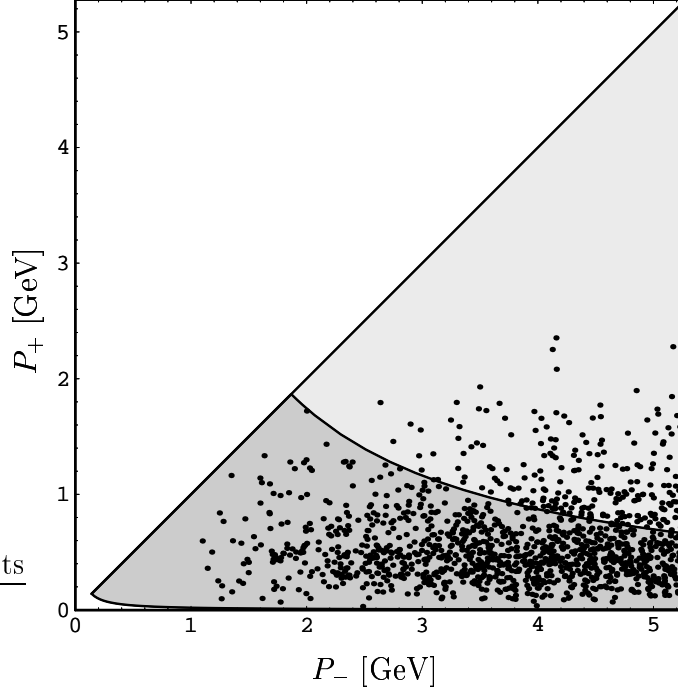


Figure 1: The hadronic phase space in  $P_+$  and  $P_-$ . Each point represents an event in a Monte-Carlo simulation using the results of this paper. While the shape-function region of large  $P_-$  and small  $P_+$  is highly populated, there is not a single event with  $P_+$  larger than 3 GeV out of the 1300 events generated.

form  $H_{ui} J \otimes \hat{S}$ , consisting of hard functions  $H_{ui}$  and the convolution of a jet function  $J$  with the leading shape function  $\hat{S}$ . More precisely,

$$\mathcal{F}_i^{(0)}(P_+, y) = H_{ui}(y, \mu_h) \int_0^{P_+} d\hat{\omega} y m_b J(y m_b (P_+ - \hat{\omega}), \mu_i) \hat{S}(\hat{\omega}, \mu_i), \quad (28)$$

where the hard functions are given by

$$H_{u1}(y, \mu_h) = 1 + \frac{C_F \alpha_s(\mu_h)}{4\pi} \left[ -4 \ln^2 \frac{y m_b}{\mu_h} + 10 \ln \frac{y m_b}{\mu_h} - 4 \ln y - \frac{2 \ln y}{1-y} - 4 L_2(1-y) - \frac{\pi^2}{6} - 12 \right],$$

$$H_{u3}(y, \mu_h) = \frac{C_F \alpha_s(\mu_h)}{4\pi} \frac{2 \ln y}{1-y}, \quad (29)$$

and  $H_{u2} = 0$ . As before, the differential decay rate is independent of the matching scales  $\mu_h \sim m_b$  and  $\mu_i \sim \sqrt{m_b \Lambda_{\text{QCD}}}$ . The jet function  $J$  has already been given in (7). Note that the  $b$ -quark mass appears only as the argument of logarithms, where it is needed to set the renormalization scales.

### 3.2 Kinematical power corrections

As in the case of  $\bar{B} \rightarrow X_s \gamma$  decay, there is a class of power corrections to the  $\bar{B} \rightarrow X_u l^- \bar{\nu}$  decay distributions which are small only because of the restriction to certain regions in phase space, but which are not associated with new hadronic parameters. In the present case, these terms can be extracted from the one-loop expressions derived in [21]. They are then convoluted with the leading shape function. As previously, the scale separation that can be achieved for these power-suppressed terms is only approximate, and we thus assign a coupling  $\alpha_s(\bar{\mu})$  with them, where the scale  $\bar{\mu}$  is expected to be of order  $\mu_i \sim \sqrt{m_b \Lambda_{\text{QCD}}}$  but is strictly not determined at this order.

The resulting expressions for the structure functions can be written in a compact form in terms of the variables  $x$  and  $y$  defined in (9) and (25). We find

$$\begin{aligned}
\mathcal{F}_1^{\text{kin}}(P_+, y) &= \frac{1}{M_B - P_+} \frac{C_F \alpha_s(\bar{\mu})}{4\pi} \int_0^{P_+} d\hat{\omega} \hat{S}(\hat{\omega}, \mu_i) \\
&\quad \times \left[ \frac{f_1(x, y)}{(1+x)^2 y(x+y)} - \frac{2g_1(x, y)}{x(1+x)^2 y^2(x+y)} \ln\left(1 + \frac{y}{x}\right) - \frac{4}{x} \ln\left(y + \frac{y}{x}\right) \right], \\
\mathcal{F}_2^{\text{kin}}(P_+, y) &= \frac{1}{M_B - P_+} \frac{C_F \alpha_s(\bar{\mu})}{4\pi} \int_0^{P_+} d\hat{\omega} \hat{S}(\hat{\omega}, \mu_i) \\
&\quad \times \left[ \frac{f_2(x, y)}{(1+x)^2 y^2(x+y)} - \frac{2x g_2(x, y)}{(1+x)^2 y^3(x+y)} \ln\left(1 + \frac{y}{x}\right) \right], \\
\mathcal{F}_3^{\text{kin}}(P_+, y) &= \frac{1}{M_B - P_+} \frac{C_F \alpha_s(\bar{\mu})}{4\pi} \int_0^{P_+} d\hat{\omega} \hat{S}(\hat{\omega}, \mu_i) \\
&\quad \times \left[ \frac{f_3(x, y)}{(1+x)^2 y^3(x+y)} + \frac{2g_3(x, y)}{(1+x)^2 y^4(x+y)} \ln\left(1 + \frac{y}{x}\right) \right], \tag{30}
\end{aligned}$$

where the functions  $f_i, g_i$  are given by

$$\begin{aligned}
f_1(x, y) &= -9y + 10y^2 + x(-16 + 12y + 6y^2) + x^2(13y - 12), \\
g_1(x, y) &= -2y^3 - 2xy^2(4 + y) - x^2y(12 + 4y + y^2) - 4x^3(y + 2) + 3x^4(y - 2), \\
f_2(x, y) &= y^2 + xy(8 + 4y + y^2) + 3x^2y(10 + y) + x^3(12 + 19y) + 10x^4, \\
g_2(x, y) &= 2y^2 + 4xy(1 + 2y) + x^2y(18 + 5y) + 6x^3(1 + 2y) + 5x^4, \\
f_3(x, y) &= 2y^3(2y - 11) + xy^2(-94 + 29y + 2y^2) + 2x^2y(-72 + 18y + 13y^2) \\
&\quad + x^3(-72 - 42y + 70y^2 - 3y^3) - 10x^4(6 - 6y + y^2), \\
g_3(x, y) &= 4y^4 - 6x(y - 5)y^3 - 4x^2y^2(-20 + 6y + y^2) + x^3y(90 - 10y - 28y^2 + y^3) \\
&\quad + x^4(36 + 36y - 50y^2 + 4y^3) + 5x^5(6 - 6y + y^2). \tag{31}
\end{aligned}$$

The above formulae are the exact  $O(\alpha_s)$  corrections to the leading-power expression. This means that, when integrated over the entire phase space, they will give rise to the correct

result for the total rate up to that order. In the shape-function region (where  $P_+ \ll P_-$ ) they can be expanded in terms of  $1/m_b$ , if desired. To this end, we count  $y = O(1)$  and  $x = O(1/m_b)$ , and expand the functions  $f_i, g_i$  in a power series in  $x$ . Note that this organizes the  $1/m_b$  expansion as an expansion in powers of the hadronic variable  $1/(M_B - P_+)$ . The leading terms in this expansion read

$$\begin{aligned}
\mathcal{F}_1^{\text{kin}(1)}(P_+, y) &= \frac{1}{M_B - P_+} \frac{C_F \alpha_s(\bar{\mu})}{4\pi} \int_0^{P_+} d\hat{\omega} \hat{S}(\hat{\omega}, \mu_i) \left[ 6 - \frac{5}{y} + \left( \frac{12}{y} - 4 \right) \ln \frac{y}{x} \right], \\
\mathcal{F}_2^{\text{kin}(1)}(P_+, y) &= \frac{1}{M_B - P_+} \frac{C_F \alpha_s(\bar{\mu})}{4\pi} \int_0^{P_+} d\hat{\omega} \hat{S}(\hat{\omega}, \mu_i) \left[ \frac{1}{y} \right], \\
\mathcal{F}_3^{\text{kin}(1)}(P_+, y) &= \frac{1}{M_B - P_+} \frac{C_F \alpha_s(\bar{\mu})}{4\pi} \int_0^{P_+} d\hat{\omega} \hat{S}(\hat{\omega}, \mu_i) \left[ 4 - \frac{22}{y} + \frac{8}{y} \ln \frac{y}{x} \right]. \tag{32}
\end{aligned}$$

Further accuracy can be achieved by adding the next-order corrections, for which we obtain

$$\begin{aligned}
\mathcal{F}_1^{\text{kin}(2)}(P_+, y) &= \frac{1}{(M_B - P_+)^2} \frac{C_F \alpha_s(\bar{\mu})}{4\pi} \int_0^{P_+} d\hat{\omega} (P_+ - \hat{\omega}) \hat{S}(\hat{\omega}, \mu_i) \\
&\quad \times \left[ -12 + \frac{16}{y} + \frac{3}{y^2} + \left( \frac{12}{y^2} - \frac{20}{y} + 6 \right) \ln \frac{y}{x} \right], \\
\mathcal{F}_2^{\text{kin}(2)}(P_+, y) &= \frac{1}{(M_B - P_+)^2} \frac{C_F \alpha_s(\bar{\mu})}{4\pi} \int_0^{P_+} d\hat{\omega} (P_+ - \hat{\omega}) \hat{S}(\hat{\omega}, \mu_i) \\
&\quad \times \left[ 1 + \frac{2}{y} + \frac{7}{y^2} - \frac{4}{y^2} \ln \frac{y}{x} \right], \\
\mathcal{F}_3^{\text{kin}(2)}(P_+, y) &= \frac{1}{(M_B - P_+)^2} \frac{C_F \alpha_s(\bar{\mu})}{4\pi} \int_0^{P_+} d\hat{\omega} (P_+ - \hat{\omega}) \hat{S}(\hat{\omega}, \mu_i) \\
&\quad \times \left[ -6 + \frac{69}{y} - \frac{64}{y^2} + \left( \frac{52}{y^2} - \frac{28}{y} \right) \ln \frac{y}{x} \right]. \tag{33}
\end{aligned}$$

In the various phase-space regions of interest to the determination of  $|V_{ub}|$ , the above terms (32) and (33) approximate the full result (30) very well (see Section 5 below).

Let us comment here on a technical point already mentioned in the Introduction. When combined with the phase-space factors in (23), the exact expressions for  $\mathcal{F}_i^{\text{kin}}$  in (30) are regular in the limit  $P_- \rightarrow P_+$ , corresponding to  $y \rightarrow 0$ . However, this feature is not automatically ensured when the structure functions, but not the phase-space factors, are expanded about the heavy-quark limit. With our choice of the variables  $x$  and  $y$ , we encounter terms as singular as  $1/y^n$  at  $n$ -th order in the expansion, as is obvious from the explicit expressions above. Phase space scales like  $y^2$  in the limit  $y \rightarrow 0$  (note that  $P_l \rightarrow P_+$  as  $P_- \rightarrow P_+$  because of (2)), so that the results (32) and (33) can be applied without encountering any kinematical singularities. In order to achieve this, it was crucial to define the variable  $y$  in the way we did in (25). We emphasize this point because straightforward application of the technology of SCET and HQET developed in [16, 31, 32] would give an expansion of the structure functions

$\mathcal{F}_i$  in powers of  $1/p_-$ , whereas phase space is proportional to  $4\vec{p}^2 = (p_- - p_+)^2 \propto y^2$ . In the kinematical region where  $p_+ < 0$ , which is allowed due to off-shell effects in the  $B$  meson, this leads to singularities as  $p_- \rightarrow 0$ . In order to avoid these singularities, we reorganize the SCET expansion as an expansion in  $1/(p_- - p_+)$  instead of  $1/p_-$ , where  $|p_+| \ll p_-$  in the shape-function region.

### 3.3 Subleading shape-function contributions

The contributions from subleading shape functions to arbitrary  $\bar{B} \rightarrow X_u l^- \bar{\nu}$  decay distributions have been derived (at tree level) in [16, 31, 32]. The result involves the same set of subleading shape functions as previously discussed in Section 2.3. Again, the structure function  $\mathcal{F}_2$  does not obtain a contribution, while

$$\begin{aligned}\mathcal{F}_1^{\text{hadr}(1)}(P_+, y) &= \frac{1}{M_B - P_+} \left[ (\bar{\Lambda} - P_+) \hat{S}(P_+) + \hat{t}(P_+) + \frac{\hat{u}(P_+) - \hat{v}(P_+)}{y} \right], \\ \mathcal{F}_3^{\text{hadr}(1)}(P_+, y) &= \frac{1}{M_B - P_+} \frac{2}{y} \left[ -(\bar{\Lambda} - P_+) \hat{S}(P_+) - 2\hat{t}(P_+) + \frac{\hat{t}(P_+) + \hat{v}(P_+)}{y} \right].\end{aligned}\quad (34)$$

At this point we recall the discussion of Section 2.3, where we have argued that the  $\bar{B} \rightarrow X_s \gamma$  photon spectrum should be used to fit the function  $\hat{S}$  of (14), which is defined to be a linear combination of the leading shape function  $\hat{S}$  and the subleading shape functions  $\hat{t}$ ,  $\hat{u}$ ,  $\hat{v}$ . Since they are the same at leading power, nothing changes in  $\mathcal{F}_i^{(0)}$  except for the simple replacement  $\hat{S} \rightarrow \hat{S}$ , which we from now on assume. At the level of subleading shape functions,  $\mathcal{F}_2^{\text{hadr}(1)} = 0$  and  $\mathcal{F}_3^{\text{hadr}(1)}$  remain unchanged, while

$$\mathcal{F}_1^{\text{hadr}(1)}(P_+, y) = \frac{1}{M_B - P_+} \left[ -(\bar{\Lambda} - P_+) \hat{S}(P_+) + 2\hat{t}(P_+) + [\hat{u}(P_+) - \hat{v}(P_+)] \left( \frac{1}{y} - 1 \right) \right]. \quad (35)$$

It follows that there reside some linear combinations of subleading shape functions in the triple differential decay rate that cannot be extracted from information on the photon spectrum in  $\bar{B} \rightarrow X_s \gamma$  decays. In the end, this dependence gives rise to a theoretical uncertainty.

### 3.4 Residual hadronic power corrections

In analogy with our treatment for the case of  $\bar{B} \rightarrow X_s \gamma$  decay, we start from the expressions for the  $1/m_b^2$  corrections to the triple differential  $\bar{B} \rightarrow X_u l^- \bar{\nu}$  decay rate obtained by applying the OPE to the hadronic tensor [12, 13]. Converting these results into the  $(n, v)$  basis and changing variables from  $v \cdot q$  and  $q^2$  to  $p_+ = n \cdot p$  and  $p_- = \bar{n} \cdot p$ , we find

$$\begin{aligned}\tilde{W}_1^{(2)} &= \delta(p_+) \left( 1 + \frac{2\lambda_1 - 3\lambda_2}{3p_-^2} \right) + \delta'(p_+) \left( \frac{2\lambda_1 - 3\lambda_2}{3p_-} - \frac{5\lambda_1 + 15\lambda_2}{6m_b} \right) - \delta''(p_+) \frac{\lambda_1}{6}, \\ \tilde{W}_2^{(2)} &= \delta(p_+) \left( -\frac{4\lambda_1 - 6\lambda_2}{3p_-^2} \right), \\ \frac{y}{4} \tilde{W}_3^{(2)} + \tilde{W}_4^{(2)} + \frac{1}{y} \tilde{W}_5^{(2)} &= \frac{\delta(p_+)}{p_-} \left( \frac{2\lambda_1 + 12\lambda_2}{3p_-} - \frac{4\lambda_1 + 9\lambda_2}{3m_b} \right) + \frac{\delta'(p_+)}{p_-} \left( \frac{2\lambda_1}{3} + 4\lambda_2 \right).\end{aligned}\quad (36)$$

The desired  $1/(M_B - P_+)^2$  corrections to the structure functions  $\mathcal{F}_i$  can then be extracted by expanding the leading and subleading contributions  $\mathcal{F}_i^{(0)}$  and  $\mathcal{F}_i^{\text{hadr}(1)}$  in terms of their moments in (18), and by subtracting the results from (36). Following the same procedure as outlined in Section 2.4 we express the result in terms of the leading shape function. This gives

$$\begin{aligned}\mathcal{F}_1^{\text{hadr}(2)}(P_+, y) &= \frac{1}{(M_B - P_+)^2} \left( \frac{4\lambda_1 - 6\lambda_2}{3y^2} - \frac{\lambda_1 + 3\lambda_2}{3} \right) \hat{S}(P_+), \\ \mathcal{F}_2^{\text{hadr}(2)}(P_+, y) &= \frac{1}{(M_B - P_+)^2} \left( \frac{-2\lambda_1 + 3\lambda_2}{3y^2} \right) \hat{S}(P_+), \\ \mathcal{F}_3^{\text{hadr}(2)}(P_+, y) &= \frac{1}{(M_B - P_+)^2} \left( \frac{4\lambda_1 + 24\lambda_2}{3y^2} - \frac{4\lambda_1 + 9\lambda_2}{3y} \right) \hat{S}(P_+).\end{aligned}\quad (37)$$

The expressions remain unchanged when the shape function  $\hat{\mathcal{S}}$  is used instead of  $\hat{S}$ .

### 3.5 Weak annihilation corrections

In the OPE calculation several contributions appear at third order in the power expansion:  $1/m_b$  corrections to the kinetic and chromo-magnetic operators, the Darwin and spin-orbit terms, and weak annihilation contributions. The Darwin and spin-orbit terms correspond to the forward  $B$ -meson matrix elements of (light) flavor-singlet operators [40]. The corresponding HQET parameters  $\rho_D^3$  and  $\rho_{LS}^3$  can in principle be extracted from inclusive  $\bar{B} \rightarrow X_c l^- \bar{\nu}$  decays. They are insensitive to the flavor of the spectator quark inside the  $B$  meson. The weak annihilation contribution, on the other hand, results from four-quark operators with flavor non-singlet structure. Graphically, this contribution corresponds to a process in which the  $b$  and  $\bar{u}$  quark annihilate into a  $W^-$ . Weak annihilation terms come with a phase-space enhancement factor of  $16\pi^2$  and so are potentially more important than other power corrections of order  $1/m_b^3$ . Because of the flavor dependence, these contributions can effect neutral and charged  $B$  mesons differently [41]. One choice of basis for the corresponding four-quark operators is [42]

$$\langle \bar{B} | \bar{b}_L \gamma_\mu u_L \bar{u}_L \gamma^\mu b_L | \bar{B} \rangle = \frac{f_B^2 M_B^2}{4} B_1, \quad \langle \bar{B} | \bar{b}_R u_L \bar{u}_L b_R | \bar{B} \rangle = \frac{f_B^2 M_B^2}{4} B_2, \quad (38)$$

where  $f_B$  is the  $B$ -meson decay constant and  $B_i$  are hadronic parameters. In the vacuum saturation approximation they are given by  $B_1 = B_2 = 1$  for charged  $B$  mesons and  $B_1 = B_2 = 0$  for neutral  $B$  mesons. The total semileptonic rate is then proportional to the difference  $B_2 - B_1$ , which implies that the weak annihilation contribution would vanish in this approximation. Currently there are only estimates of the magnitude of the deviation of this difference from zero, but its effect of the total branching ratio is [43]

$$\delta B(\bar{B} \rightarrow X_u l^- \bar{\nu}) \approx 3.9 \left( \frac{f_B}{0.2 \text{ GeV}} \right)^2 \left( \frac{B_2 - B_1}{0.1} \right) |V_{ub}|^2. \quad (39)$$

Again, we expect this effect to be different for charged and neutral  $B$  mesons. The most important feature of weak annihilation is that it is formally concentrated at the kinematical

point where all the momentum of the heavy quark is transferred to the lepton pair [41]. At the parton level this implies that the corresponding contribution is proportional to  $\delta(q^2 - m_b^2)$ . It is therefore included in every cut that includes the  $q^2$  endpoint, and its effect is independent of the specific form of the cut.

We suggest two different strategies to control this effect. The first is to include it in the error estimate as a constant contribution proportional to the total rate. A recent study [44] puts a limit on this effect of  $\pm 1.8\%$  on the total rate (at 68% confidence level) by analyzing CLEO data. The second one is to impose a cut  $q^2 \leq q_{\text{max}}^2$ , thus avoiding the region where the weak annihilation contribution is concentrated. The maximal value of  $q^2$  is  $(M_B - M_\pi)^2$ , but one must exclude a larger region of phase space, such that the *excluded* portion at large  $q^2$  (corresponding to a region near the origin in the  $(P_-, P_+)$  plane) can be reliably calculated. In our numerical analysis, we will study the effect of a cut  $q^2 \leq (M_B - M_D)^2$ , which satisfies this criterion.

For completeness, we note that even after the weak annihilation contribution near maximum  $q^2$  has been removed, there could in principle exist other, flavor-specific contributions to the semileptonic decay amplitudes that are different for charged and neutral  $B$  mesons. The leading terms of this kind contribute at order  $1/m_b$  in the shape-function region and are parameterized by a set of four-quark subleading shape functions [16, 31]. Model estimates of these contributions show that they are very small for all observables considered for an extraction of  $|V_{ub}|$  [32, 45]. If only flavor-averaged decay rates are measured, the effects of four-quark subleading shape functions can be absorbed entirely by a redefinition of the functions  $\hat{u}(\hat{\omega})$  and  $\hat{v}(\hat{\omega})$  [16], without affecting the moment relations in (18).

## 4 Shape-function parameterizations

Hadronic-physics effects enter the description of inclusive decay rates via non-perturbative shape functions. Perturbation theory cannot tell us much about the local form of these functions, but moments of them are calculable provided that the domain of integration is much larger than  $\Lambda_{\text{QCD}}$ . Since the shape functions contain much information about the internal structures of the  $b$  quark inside the  $B$  meson, knowledge of them relates directly to the determination of the  $b$ -quark mass  $m_b$ , the kinetic energy  $\lambda_1$ , and, in principle, the matrix elements of higher-dimensional operators. Improved measurements of the shape of the  $\bar{B} \rightarrow X_s \gamma$  photon spectrum will therefore lead directly to a more precise determination of HQET parameters. This argument can be turned around to constrain the leading shape function using knowledge of  $m_b$  and  $\lambda_1$  from other physical processes such as a  $b \rightarrow c$  moment analysis [46]. We emphasize, however, that there are obviously infinitely many locally different functions that have identical first few moments. In this section we present a few functional forms that can be used to model the shape functions and to fit the current experimental data.

To achieve stringent constraints on the leading shape function a precise definition of the HQET parameters is required. It is a well-known fact that the pole-mass scheme introduces uncontrollable ambiguities. To avoid these uncertainties several short-distance definitions have been proposed, such as the  $\overline{\text{MS}}$  scheme, the potential-subtraction scheme [47], the  $\Upsilon(1S)$  scheme [48], the kinetic scheme [49], or the shape-function scheme [9]. While the decay rates

are of course independent of the particular choice, it is advantageous to use a mass scheme that is designed for the physics problem at hand. In the case of inclusive  $B$  decays into light particles, this is the shape-function scheme.

## 4.1 Models for the leading shape function

### 4.1.1 Moment relations in the shape-function scheme

Moments of  $\hat{S}(\hat{\omega}, \mu_i)$  are defined with an upper limit of integration  $\hat{\omega}_0$ . For practical applications,  $\hat{\omega}_0$  should be thought of as the size of the window where the  $\bar{B} \rightarrow X_s \gamma$  photon spectrum is experimentally accessible, e.g.  $\hat{\omega}_0 = M_B - 2E_\gamma^{\min}$  with  $E_\gamma^{\min} \approx 1.8 \text{ GeV}$ . Following [9], we define

$$M_N(\hat{\omega}_0, \mu_i) \equiv \int_0^{\hat{\omega}_0} d\hat{\omega} \hat{\omega}^N \hat{S}(\hat{\omega}, \mu_i). \quad (40)$$

These moments can be expanded in terms of matrix elements of local operators as long as  $\hat{\omega}_0$  is much larger than  $\Lambda_{\text{QCD}}$ . The shape-function scheme defines these HQET parameters implicitly through the moment relations to all orders in perturbation theory,

$$\begin{aligned} \frac{M_1(\mu_f + \bar{\Lambda}(\mu_f, \mu_i), \mu_i)}{M_0(\mu_f + \bar{\Lambda}(\mu_f, \mu_i), \mu_i)} &= \bar{\Lambda}(\mu_f, \mu_i), \\ \frac{M_2(\mu_f + \bar{\Lambda}(\mu_f, \mu_i), \mu_i)}{M_0(\mu_f + \bar{\Lambda}(\mu_f, \mu_i), \mu_i)} &= \frac{\mu_\pi^2(\mu_f, \mu_i)}{3} + \bar{\Lambda}^2(\mu_f, \mu_i), \end{aligned} \quad (41)$$

etc. Here, the factorization scale  $\mu_f \gg \Lambda_{\text{QCD}}$  is related to the size of the integration domain via the implicit equation  $\hat{\omega}_0 = \mu_f + \bar{\Lambda}(\mu_f, \mu_i)$ . In practice  $\mu_f$  is close to the intermediate scale  $\mu_i$ . At tree level, the relations between parameters in the shape-function scheme and the pole scheme are  $\bar{\Lambda}(\mu_f, \mu_i) = \bar{\Lambda}^{\text{pole}}$ ,  $\mu_\pi^2(\mu_f, \mu_i) = -\lambda_1$ , etc. They have been worked out to two-loop order in [50], which allows for a precise determination of  $\bar{\Lambda}(\mu_f, \mu_i)$  and  $\mu_\pi^2(\mu_f, \mu_i)$  from other physical processes.

For reference purposes, it is helpful to quote values for the  $\bar{\Lambda}$  and  $\mu_\pi^2$  using only a single scale  $\mu_*$  instead of two independent scales  $\mu_f$  and  $\mu_i$ . To one-loop order, these parameters can be related to those determined from the moments via [9]

$$\bar{\Lambda}(\mu_*, \mu_*) = \bar{\Lambda}(\mu_f, \mu_i) + \mu_* \frac{C_F \alpha_s(\mu_*)}{\pi} - \mu_f \frac{C_F \alpha_s(\mu_i)}{\pi} \left[ 1 - 2 \left( 1 - \frac{\mu_\pi^2(\mu_f, \mu_i)}{3\mu_f^2} \right) \ln \frac{\mu_f}{\mu_i} \right], \quad (42)$$

$$\mu_\pi^2(\mu_*, \mu_*) = \mu_\pi^2(\mu_f, \mu_i) \left[ 1 + \frac{C_F \alpha_s(\mu_*)}{2\pi} - \frac{C_F \alpha_s(\mu_i)}{\pi} \left( \frac{1}{2} + 3 \ln \frac{\mu_f}{\mu_i} \right) \right] + 3\mu_f^2 \frac{C_F \alpha_s(\mu_i)}{\pi} \ln \frac{\mu_f}{\mu_i},$$

where we have neglected higher-dimensional operator matrix elements that are suppressed by inverse powers of  $\mu_f$ . A typical choice for the scale  $\mu_*$  is 1.5 GeV, which we will use as the reference scale throughout this work. It will be convenient to connect the parameter  $\bar{\Lambda}$  extracted from the first moment of the shape function with a low-scale subtracted quark-mass definition referred to as the ‘‘shape-function’’ mass. Following [9], we define

$$m_b(\mu_f, \mu_i) \equiv M_B - \bar{\Lambda}(\mu_f, \mu_i). \quad (43)$$

The general procedure for modeling the leading shape function  $\hat{S}(\hat{\omega}, \mu_i)$  from a given functional form  $F(\hat{\omega})$  is as follows. The shape of  $F(\hat{\omega})$  is assumed to be tunable so that it can be used to fit the  $\bar{B} \rightarrow X_s \gamma$  photon spectrum. Only the norm of the shape function remains to be fixed. Note that the moment relations (41) are insensitive to the norm, so that formulae for  $\bar{\Lambda}$  and  $\mu_\pi^2$  follow directly from the functional form of  $F(\hat{\omega})$ . Examples of such formulae will be given below. We define moments  $M_N^{[F]}(\hat{\omega}_0)$  of  $F$  in analogy with (40). The first relation in (41) implies that for a given  $\hat{\omega}_0$  the factorization scale is

$$\mu_f = \hat{\omega}_0 - \frac{M_1^{[F]}(\hat{\omega}_0)}{M_0^{[F]}(\hat{\omega}_0)}. \quad (44)$$

Now that  $\mu_f$  is known, the norm is determined by requiring that the zeroth moment of the shape function is [9]

$$M_0(\hat{\omega}_0, \mu_i) = 1 - \frac{C_F \alpha_s(\mu_i)}{\pi} \left( \ln^2 \frac{\mu_f}{\mu_i} + \ln \frac{\mu_f}{\mu_i} + \frac{\pi^2}{24} \right) + \frac{C_F \alpha_s(\mu_i)}{\pi} \left( \ln \frac{\mu_f}{\mu_i} - \frac{1}{2} \right) \frac{\mu_\pi^2(\mu_f, \mu_i)}{3\mu_f^2} + \dots \quad (45)$$

It follows that  $[M_0(\hat{\omega}_0, \mu_i)/M_0^{[F]}(\hat{\omega}_0)] F(\hat{\omega})$  serves as a model of  $\hat{S}(\hat{\omega}, \mu_i)$  or  $\hat{\mathcal{S}}(\hat{\omega}, \mu_i)$ .

#### 4.1.2 Three models

We will now suggest three two-parameter models for the leading-order shape function based on an exponential-type function  $F^{(\text{exp})}$ , a gaussian-type function  $F^{(\text{gauss})}$ , and hyperbolic-type function  $F^{(\text{hyp})}$ . We use two parameters that can be tuned to fit the photon spectrum: a dimensionful quantity  $\Lambda$  which coincides with the position of the average  $\langle \hat{\omega} \rangle$ , and a positive number  $b$  which governs the behavior for small  $\hat{\omega}$ . They are

$$\begin{aligned} F^{(\text{exp})}(\hat{\omega}; \Lambda, b) &= \frac{N^{(\text{exp})}}{\Lambda} \left( \frac{\hat{\omega}}{\Lambda} \right)^{b-1} \exp \left( -d_{(\text{exp})} \frac{\hat{\omega}}{\Lambda} \right), \\ F^{(\text{gauss})}(\hat{\omega}; \Lambda, b) &= \frac{N^{(\text{gauss})}}{\Lambda} \left( \frac{\hat{\omega}}{\Lambda} \right)^{b-1} \exp \left( -d_{(\text{gauss})} \frac{\hat{\omega}^2}{\Lambda^2} \right), \\ F^{(\text{hyp})}(\hat{\omega}; \Lambda, b) &= \frac{N^{(\text{hyp})}}{\Lambda} \left( \frac{\hat{\omega}}{\Lambda} \right)^{b-1} \cosh^{-1} \left( d_{(\text{hyp})} \frac{\hat{\omega}}{\Lambda} \right). \end{aligned} \quad (46)$$

For convenience, we normalize these functions to unity. The parameters  $d_{(i)}$  are determined by the choice  $\Lambda = \langle \hat{\omega} \rangle$ . For given parameters  $\Lambda$  and  $b$  we find

$$\begin{aligned} N^{(\text{exp})} &= \frac{d_{(\text{exp})}^b}{\Gamma(b)}, & d_{(\text{exp})} &= b, \\ N^{(\text{gauss})} &= \frac{2d_{(\text{gauss})}^{b/2}}{\Gamma(b/2)}, & d_{(\text{gauss})} &= \left( \frac{\Gamma(\frac{1+b}{2})}{\Gamma(\frac{b}{2})} \right)^2, \\ N^{(\text{hyp})} &= \frac{[4d_{(\text{hyp})}]^b}{2\Gamma(b) [\zeta(b, \frac{1}{4}) - \zeta(b, \frac{3}{4})]}, & d_{(\text{hyp})} &= \frac{b}{4} \frac{\zeta(1+b, \frac{1}{4}) - \zeta(1+b, \frac{3}{4})}{\zeta(b, \frac{1}{4}) - \zeta(b, \frac{3}{4})}, \end{aligned} \quad (47)$$

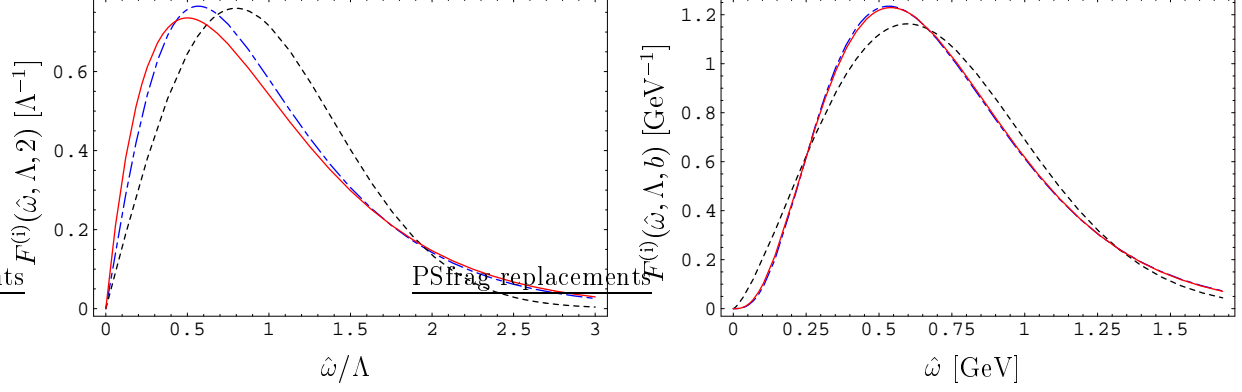


Figure 2: LEFT: Different functional forms for the leading shape function. We show  $F^{(\text{exp})}(\hat{\omega}, \Lambda, 2)$  (solid),  $F^{(\text{gauss})}(\hat{\omega}, \Lambda, 2)$  (dotted), and  $F^{(\text{hyp})}(\hat{\omega}, \Lambda, 2)$  (dash-dotted). RIGHT: The same functions with the parameters  $\Lambda$  and  $b$  tuned such that  $m_b(\mu_*, \mu_*) = 4.61 \text{ GeV}$  and  $\mu_\pi^2(\mu_*, \mu_*) = 0.2 \text{ GeV}^2$ . See text for explanation.

where  $\zeta(b, a) = \sum_{k=0}^{\infty} (k+a)^{-b}$  is the generalized Riemann zeta function. An illustration of the functional forms of the models is given on the left-hand side in Figure 2. We show a plot with the choice  $b = 2$ , corresponding to a linear onset for small  $\hat{\omega}$ .

For the first two models, analytic expressions for the HQET parameters  $\bar{\Lambda}$  and  $\mu_\pi^2$  are available. Following the discussion above, we compute the moments over the interval  $[0, \hat{\omega}_0]$  and find for the exponential form  $F^{(\text{exp})}(\hat{\omega}; \Lambda, b)$

$$\begin{aligned} \bar{\Lambda}(\mu_f, \mu_i) &= \frac{\Lambda}{b} \frac{\Gamma(1+b) - \Gamma(1+b, \frac{b\hat{\omega}_0}{\Lambda})}{\Gamma(b) - \Gamma(b, \frac{b\hat{\omega}_0}{\Lambda})}, \\ \mu_\pi^2(\mu_f, \mu_i) &= 3 \left[ \frac{\Lambda^2}{b^2} \frac{\Gamma(2+b) - \Gamma(2+b, \frac{b\hat{\omega}_0}{\Lambda})}{\Gamma(b) - \Gamma(b, \frac{b\hat{\omega}_0}{\Lambda})} - \bar{\Lambda}(\mu_f, \mu_i)^2 \right], \end{aligned} \quad (48)$$

where  $\mu_f = \hat{\omega}_0 - \bar{\Lambda}(\mu_f, \mu_i)$ . A similar calculation for the Gaussian form  $F^{(\text{gauss})}(\hat{\omega}; \Lambda, b)$  yields

$$\begin{aligned} \bar{\Lambda}(\mu_f, \mu_i) &= \frac{\Lambda}{\sqrt{d_{(\text{gauss})}}} \frac{\Gamma(\frac{1+b}{2}) - \Gamma(\frac{1+b}{2}, \frac{d_{(\text{gauss})}\hat{\omega}_0^2}{\Lambda^2})}{\Gamma(\frac{b}{2}) - \Gamma(\frac{b}{2}, \frac{d_{(\text{gauss})}\hat{\omega}_0^2}{\Lambda^2})}, \\ \mu_\pi^2(\mu_f, \mu_i) &= 3 \left[ \frac{\Lambda^2}{d_{(\text{gauss})}} \frac{\Gamma(1+\frac{b}{2}) - \Gamma(1+\frac{b}{2}, \frac{d_{(\text{gauss})}\hat{\omega}_0^2}{\Lambda^2})}{\Gamma(\frac{b}{2}) - \Gamma(\frac{b}{2}, \frac{d_{(\text{gauss})}\hat{\omega}_0^2}{\Lambda^2})} - \bar{\Lambda}(\mu_f, \mu_i)^2 \right]. \end{aligned} \quad (49)$$

For the hyperbolic form  $F^{(\text{hyp})}(\hat{\omega}; \Lambda, b)$  the procedure can be performed numerically.

Ultimately the shape function should be fitted to the  $\bar{B} \rightarrow X_s \gamma$  photon spectrum, and the above equations then determine  $\bar{\Lambda}$  and  $\mu_\pi^2$ . On the other hand, these formulae can be inverted to determine  $\Lambda$  and  $b$  from the current values of the HQET parameters. For example, if we were to adopt the values  $m_b(\mu_*, \mu_*) = 4.61 \text{ GeV}$  and  $\mu_\pi^2(\mu_*, \mu_*) = 0.20 \text{ GeV}^2$  for the parameters

in (42) at  $\mu_* = 1.5 \text{ GeV}$ , we would find the parameter pair  $\Lambda \approx 0.72 \text{ GeV}$ ,  $b \approx 3.95$  for the exponential model,  $\Lambda \approx 0.71 \text{ GeV}$ ,  $b \approx 2.36$  for the gaussian model, and  $\Lambda \approx 0.73 \text{ GeV}$ ,  $b \approx 3.81$  for the hyperbolic model. On the right-hand side of Figure 2 we show these three different curves, plotted over the interval  $[0, \hat{\omega}_0]$ , over which the moment constraints are imposed. While the exponential curve (solid) and the hyperbolic function (dash-dotted) are barely distinguishable, the gaussian model has quite different characteristics. It is broader, almost linear at the onset, faster to fall off, and the maximum is shifted toward larger  $\hat{\omega}$ .

In most applications, shape functions are needed for arguments  $\hat{\omega}$  of order  $\Lambda_{\text{QCD}}$ . However, in some cases, like the ideal cut on hadronic invariant mass,  $\hat{\omega}$  is required to be as large as  $M_D$ , which is much larger than  $\Lambda_{\text{QCD}}$ . The large- $\hat{\omega}$  behavior of the shape functions can be computed in a model-independent way using short-distance methods [9]. For the leading shape function, one finds

$$\hat{S}(\hat{\omega} \gg \Lambda_{\text{QCD}}, \mu_i) = -\frac{C_F \alpha_s(\mu_i)}{\pi} \frac{1}{\hat{\omega} - \bar{\Lambda}} \left( 2 \ln \frac{\hat{\omega} - \bar{\Lambda}}{\mu_i} + 1 \right) + \dots \quad (50)$$

Note that this radiative tail is negative, implying that the shape function must go through zero somewhere near  $\hat{\omega} \sim \text{few } \Lambda_{\text{QCD}}$ . For practical purposes, we “glue” the above expression onto models of the non-perturbative shape function starting at  $\hat{\omega} = \bar{\Lambda} + \mu_i/\sqrt{e} \approx 1.6 \text{ GeV}$ , where the tail piece vanishes. In this way we obtain a continuous shape-function model with the correct asymptotic behavior. We stress that for applications with a maximal  $P_+$  not larger than about  $1.6 \text{ GeV}$  the radiative tail of the shape function is never required. This includes all methods for extracting  $|V_{ub}|$  discussed later in this work, except for the case of a cut on hadronic invariant mass,  $M_X \leq M_0$ , if  $M_0$  is above  $1.6 \text{ GeV}$ .

## 4.2 Models for subleading shape functions

In the last section we have been guided by the fact that the  $\bar{B} \rightarrow X_s \gamma$  photon spectrum is at leading power directly determined by the leading shape function. This helped in finding models that have roughly the same shape as the photon spectrum. At the subleading level considered here, however, no such guidance is provided to us. The available information is limited to the tree-level moment relations (18), stating that the norms of the subleading shape functions vanish while their first moments do not. In [16], two classes of models have been proposed, in which the subleading shape functions are “derived” from the leading shape function. This procedure yields the following forms:

$$\hat{t}_1(\hat{\omega}) = \frac{3\lambda_2}{\lambda_1} (\bar{\Lambda} - \hat{\omega}) \hat{S}(\hat{\omega}), \quad \hat{u}_1(\hat{\omega}) = -2(\bar{\Lambda} - \hat{\omega}) \hat{S}(\hat{\omega}), \quad \hat{v}_1(\hat{\omega}) = -\frac{3\lambda_2}{\lambda_1} (\bar{\Lambda} - \hat{\omega}) \hat{S}(\hat{\omega}), \quad (51)$$

and

$$\hat{t}_2(\hat{\omega}) = -\lambda_2 \hat{S}'(\hat{\omega}), \quad \hat{u}_2(\hat{\omega}) = \frac{2\lambda_1}{3} \hat{S}'(\hat{\omega}), \quad \hat{v}_2(\hat{\omega}) = \lambda_2 \hat{S}'(\hat{\omega}). \quad (52)$$

Below, we will sometimes refer to the first set of functions as the “default choice”.

For consistency with the tree-level moment relations, we choose the parameters  $\bar{\Lambda}$  and  $-\lambda_1$  in the expressions for the subleading shape functions (as well as in the expressions for the

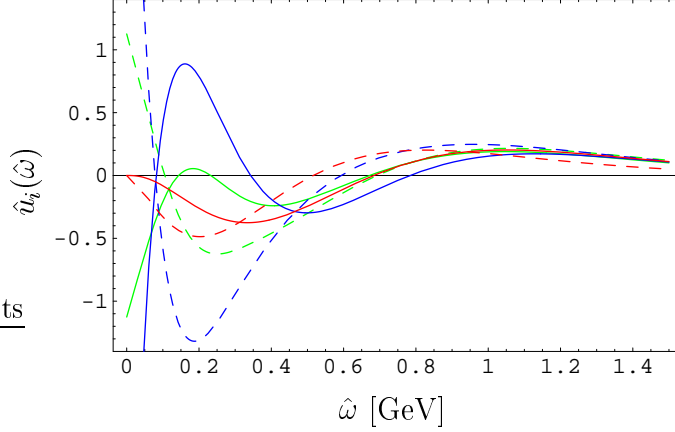


Figure 3: Six models for the subleading shape function  $\hat{u}(\hat{\omega})$ . We use  $M_2 = (0.3 \text{ GeV})^3$  in all cases. The parameter  $a = 5$  for the function  $h^{(N)}$ , and  $a = 10$  for the function  $h^{(\text{BIK})}$ . See text for explanation.

second-order hadronic power corrections) to coincide with the expressions for  $\bar{\Lambda}(\mu_f, \mu_i)$  and  $\mu_\pi^2(\mu_f, \mu_i)$  given in (48) and (49) in the limit where  $\omega_0 \rightarrow \infty$ . This ensures, in particular, that the subleading shape functions have zero norm when integrated over  $0 \leq \hat{\omega} < \infty$ . For the model functions in (46), we obtain in all three cases  $\bar{\Lambda} = \Lambda$ , and

$$-\lambda_1 = \left\{ \frac{1}{b}, \frac{\Gamma(1 + \frac{b}{2}) \Gamma(\frac{b}{2})}{\Gamma(\frac{1+b}{2})^2} - 1, \frac{1+b}{b} \frac{[\zeta(b, \frac{1}{4}) - \zeta(b, \frac{3}{4})][\zeta(2+b, \frac{1}{4}) - \zeta(2+b, \frac{3}{4})]}{[\zeta(1+b, \frac{1}{4}) - \zeta(1+b, \frac{3}{4})]^2} - 1 \right\} \quad (53)$$

for the three models, respectively.

There are of course infinitely many possibilities to find models for subleading shape functions that are in accordance with (18). Any function with vanishing norm and first moment (defined with respect to the variable  $\omega$ ) can be arbitrarily added to any model for a subleading shape function without violating the moment relations. Several such functions have been proposed in recent work on subleading shape functions, see e.g. [16, 30, 32, 45]. Specifically, let us define

$$\begin{aligned} h^{(N)}(\hat{\omega}) &\equiv \frac{M_2}{N\Omega_0^3} \left\{ \frac{a^3}{2} e^{-az} \left( 1 - 2az + \frac{a^2 z^2}{2} \right) \right\}, \\ h^{(\text{GN})}(\hat{\omega}) &\equiv \frac{M_2}{N\Omega_0^3} \left\{ \left[ \frac{2\sqrt{\pi a}}{\pi - 2} e^{-az^2} \left( 1 - 2z\sqrt{\frac{a}{\pi}} \right) \right] - 2e^{-z} + 2z e^{-2z} \text{Ei}(z) \right\}, \\ h^{(\text{BIK})}(\hat{\omega}) &\equiv \frac{M_2}{N\Omega_0^3} \left\{ \left[ \frac{\pi^2}{4} \frac{2\sqrt{\pi a}}{\pi - 2} e^{-az^2} \left( 1 - 2z\sqrt{\frac{a}{\pi}} \right) \right] \right. \\ &\quad \left. + \frac{8}{(1+z^2)^4} \left[ z \ln z + \frac{z}{2} (1+z^2) - \frac{\pi}{4} (1-z^2) \right] \right\}, \end{aligned} \quad (54)$$

where  $z = \hat{\omega}/\Omega_0$ , and the reference quantity  $\Omega_0 = O(\Lambda_{\text{QCD}})$  depends on the type of function,

namely  $\Omega_0 = \bar{\Lambda}$  for  $h^{(N)}$ ,  $\Omega_0 = \frac{2}{3}\bar{\Lambda}$  for  $h^{(\text{GN})}$ , and  $\Omega_0 = \frac{8}{3\pi}\bar{\Lambda}$  for  $h^{(\text{BIK})}$ . The quantity  $a$  is a free parameter. The functions (54) have by construction vanishing norm and first moment. Their second moments are given by the parameter  $M_2$ , provided the normalization constants are chosen as  $N = 1$  for  $h^{(N)}$ , and

$$N = 1 - \frac{4 - \pi}{2(\pi - 2)} \frac{1}{a}, \quad N = 1 - \frac{\pi^2(4 - \pi)}{8(\pi - 2)} \frac{1}{a} \quad (55)$$

for  $h^{(\text{GN})}$  and  $h^{(\text{BIK})}$ , respectively. The values for the parameters  $a$  and  $M_2$  should be chosen such that the following characteristics of subleading shape functions are respected: First, they are dimensionless functions, so that their values are naturally of  $O(1)$  for  $\hat{\omega} \sim \Lambda_{\text{QCD}}$ . Secondly, when integrated over a sufficiently large domain, their contributions are determined in terms of their first few moments. In particular, this implies that for values of  $\hat{\omega} \gg \Lambda_{\text{QCD}}$  the integrals over the subleading shape functions must approach zero.

Given the three functions (54), we can construct several new sets of models of the form  $\{\hat{t} \pm h^{(i)}, \hat{u} \pm h^{(i)}, \hat{v} \pm h^{(i)}\}$ . Specifically, we use the following four new sets of subleading shape-function models:

$$\begin{aligned} \hat{t}_3(\hat{\omega}) &= \hat{t}_1(\hat{\omega}) - h^{(N)}(\hat{\omega}), & \hat{u}_3(\hat{\omega}) &= \hat{u}_1(\hat{\omega}) + h^{(N)}(\hat{\omega}), & \hat{v}_3(\hat{\omega}) &= \hat{v}_1(\hat{\omega}) - h^{(N)}(\hat{\omega}), \\ \hat{t}_4(\hat{\omega}) &= \hat{t}_1(\hat{\omega}) + h^{(N)}(\hat{\omega}), & \hat{u}_4(\hat{\omega}) &= \hat{u}_1(\hat{\omega}) - h^{(N)}(\hat{\omega}), & \hat{v}_4(\hat{\omega}) &= \hat{v}_1(\hat{\omega}) + h^{(N)}(\hat{\omega}), \\ \hat{t}_5(\hat{\omega}) &= \hat{t}_1(\hat{\omega}) - h^{(\text{BIK})}(\hat{\omega}), & \hat{u}_5(\hat{\omega}) &= \hat{u}_1(\hat{\omega}) + h^{(\text{BIK})}(\hat{\omega}), & \hat{v}_5(\hat{\omega}) &= \hat{v}_1(\hat{\omega}) - h^{(\text{BIK})}(\hat{\omega}), \\ \hat{t}_6(\hat{\omega}) &= \hat{t}_1(\hat{\omega}) + h^{(\text{BIK})}(\hat{\omega}), & \hat{u}_6(\hat{\omega}) &= \hat{u}_1(\hat{\omega}) - h^{(\text{BIK})}(\hat{\omega}), & \hat{v}_6(\hat{\omega}) &= \hat{v}_1(\hat{\omega}) + h^{(\text{BIK})}(\hat{\omega}). \end{aligned} \quad (56)$$

Using the function  $h^{(\text{GN})}$  instead of  $h^{(N)}$  or  $h^{(\text{BIK})}$  would lead to smaller variations. Note that for these choices we no longer have  $\hat{t}(\hat{\omega}) = -\hat{v}(\hat{\omega})$ , which was an ‘‘accidental’’ feature of the first two models (51) and (52). The fact that the two functions have equal (but opposite in sign) first moments does not imply that their higher moments should also be related to each other.

We display the six different models for  $\hat{u}(\hat{\omega})$  in Figure 3, where we have used the exponential-type model (46) for  $\hat{S}(\hat{\omega})$ . In the region  $\hat{\omega} \sim \Lambda_{\text{QCD}}$  they differ dramatically from each other, while the large  $\hat{\omega}$  dependence is dominated by the moment relations (18). In practice we shall use this set of models to estimate the dependence of rates on subleading shape functions.

### 4.3 Illustrative studies and embellishments

We stressed several times that the calculation of the hadronic tensor is ‘‘optimized’’ for the shape-function region of large  $P_-$  and small  $P_+$ , while it can smoothly be extended over the entire phase space. The notions ‘‘large  $P_-$ ’’ and ‘‘small  $P_+$ ’’ are to be understood as the sizes of integration domains for  $P_-$  and  $P_+$ . When the differential distributions are integrated over a sufficiently large region in phase space, global quark-hadron duality ensures that the partonic description used in the present work matches the true, hadronic distributions with good accuracy. A more ambitious goal would be to calculate the differential decay rate point by point in the  $(P_+, P_-)$  plane. This can be done invoking local quark-hadron duality, as long as there is a sufficiently large number of hadronic final-state resonances contributing to the rate at any given point in phase space.

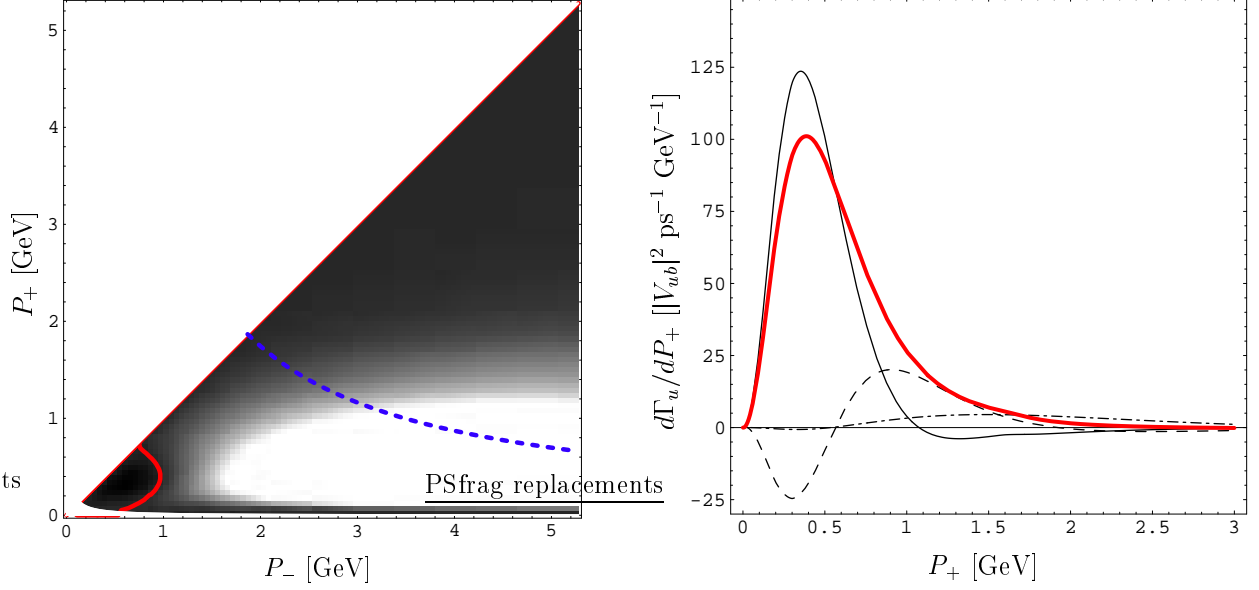


Figure 4: **LEFT:** Theoretical prediction for the double differential decay rate. The light area represents a large and positive decay rate. Black regions denote areas where the decay rate is close to zero. The dotted line is given by  $P_+ P_- = M_D^2$ , which means that charmed background is located in the upper wedge. See text for further explanation. **RIGHT:** The  $P_+$  spectrum extended to large values of  $P_+$ . The thin solid line denotes the leading-power prediction, the dashed line depicts first-order power corrections, and the dash-dotted line second-order power corrections. The thick solid line is their sum.

It is instructive to integrate the triple differential decay rate (23) over the leptonic variable  $P_+ \leq P_l \leq P_-$ , which yields the exact formula

$$\frac{d^2\Gamma_u}{dP_+ dP_-} = \frac{G_F^2 |V_{ub}|^2}{96\pi^3} U_y(\mu_h, \mu_i) (M_B - P_+) (P_- - P_+)^2 \times \left\{ (3M_B - 2P_- - P_+) \mathcal{F}_1 + 6(M_B - P_-) \mathcal{F}_2 + (P_- - P_+) \mathcal{F}_3 \right\}. \quad (57)$$

Our theoretical prediction for the double differential decay rate (57) is shown on the left-hand side of Figure 4. We use the exponential model for the leading shape function with parameters  $m_b(\mu_*, \mu_*) = 4.61 \text{ GeV}$  and  $\mu_\pi^2(\mu_*, \mu_*) = 0.2 \text{ GeV}^2$ , as well as the default choice (model 1) for the subleading shape functions. For very small  $P_-$  values the rate turns negative (to the left of the red line in the figure), signaling a breakdown of quark-hadron duality. It is reassuring that the only region where this happens is the “resonance region”, where the hadronic invariant mass is of order  $\Lambda_{\text{QCD}}$ , and local duality breaks down.

Another useful quantity to consider is the differential  $P_+$  rate, which is obtained by integrating the double differential rate over  $P_+ \leq P_- \leq M_B$ . We plot the resulting  $P_+$  spectrum over a large domain, which is shown on the right-hand side of Figure 4. In the plot we also disentangle the contributions from different orders in power counting.

## 5 Predictions and error estimates for partial rates

Before discussing predictions for partial  $\bar{B} \rightarrow X_u l^- \bar{\nu}$  rates for various experimental cuts, let us recapitulate the ingredients of the calculation and general procedure. We have presented expressions for the triple differential decay rate, which can be organized in an expansion in inverse powers of  $(M_B - P_+)$ . The leading-power contribution is given at next-to-leading order in renormalization-group improved perturbation theory. At first subleading power two contributions arise. The first type involves subleading shape functions and is included at tree level, while the second type contributes perturbative corrections of order  $\alpha_s$  that come with the leading shape function. Further contributions enter at second subleading power and are again of the two types: perturbative corrections of order  $\alpha_s$  and non-perturbative structures at tree level. In summary, then, partial rates are computed term by term in an expansion of the form

$$\Gamma_u = \Gamma_u^{(0)} + (\Gamma_u^{\text{kin}(1)} + \Gamma_u^{\text{hadr}(1)}) + (\Gamma_u^{\text{kin}(2)} + \Gamma_u^{\text{hadr}(2)}) + \dots \quad (58)$$

The goal of this section is to test the convergence of this series and to perform a thorough analysis of uncertainties. For the kinematical corrections  $\Gamma_u^{\text{kin}(n)}$  the sum of all terms is known and given by the expressions in (30), while the first two terms in the series correspond to the expanded results in (32) and (33). We will find that in all cases of interest the first two terms given an excellent approximation to the exact result for  $\Gamma_u^{\text{kin}}$ .

For the purpose of illustration, we adopt the exponential model for the shape function and present numerical results for two sets of input parameters, which are biased by the results deduced from experimental fits to  $\bar{B} \rightarrow X_c l^- \bar{\nu}$  moments, as discussed in [50]. Specifically, we use  $m_b(\mu_*, \mu_*) = 4.61 \text{ GeV}$ ,  $\mu_\pi^2(\mu_*, \mu_*) = 0.2 \text{ GeV}^2$  (set 1) and  $m_b(\mu_*, \mu_*) = 4.55 \text{ GeV}$ ,  $\mu_\pi^2(\mu_*, \mu_*) = 0.3 \text{ GeV}^2$  (set 2). The values of the  $b$ -quark mass coincide with those obtained at two-loop and one-loop order in [50] (see also the discussion below), while the values of  $\mu_\pi^2$  are close to the corresponding values in that reference. As was mentioned before, in the future the leading shape function  $\hat{\mathcal{S}}(\hat{\omega}, \mu_i)$  should be extracted from a fit to the  $\bar{B} \rightarrow X_s \gamma$  photon spectrum, in which case the uncertainty in its shape becomes an experimental error, which can be systematically reduced with better and better data. In the process, the “theoretically preferred” parameter values used in the present work will be replaced with the “true” values extracted directly from data. While this will change the central values for the partial rates, our estimates of the remaining theoretical errors will only be affected marginally.

The different sources of theoretical uncertainties are as follows: First, there are uncertainties associated with the functional forms of the subleading shape functions. To estimate them, we take the spread of results when using the six different models of Section 4.2, while the central value for a partial decay rate corresponds to the average over the different models. Secondly, there are perturbative uncertainties associated with the setting of the matching scales  $\mu_h$ ,  $\mu_i$ , and  $\bar{\mu}$ . Decay rates are formally independent of them, but a residual dependence remains because of the truncation of the perturbative series. Our error analysis is as follows:

- The hard scale  $\mu_h$  is of order  $m_b$ . In perturbative logarithms the scale appears in the combination  $(y m_b / \mu_h)$ , see e.g. (29). To set a central value for  $\mu_h$  we are guided by the average  $\langle y \rangle m_b$ . The leading term for the double differential decay rate  $d^2 \Gamma_u / dP_+ dy$  is proportional to  $2y^2(3 - 2y)$ . It follows that the average  $y$  on the interval  $[0, 1]$  is 0.7.

However, in some applications  $y$  is not integrated over the full domain. Also, there are large negative constants in the matching correction  $H_{u1}$  in (29), whose effect can be ameliorated by lowering the scale further. In the error analysis we use the central value of  $\mu_h = m_b/2 \approx 2.3 \text{ GeV}$  and vary the scale by a factor between  $1/\sqrt{2}$  and  $\sqrt{2}$ . For the central value  $\alpha_s(\mu_h) \approx 0.286$ .

- The intermediate scale  $\mu_i \sim \sqrt{m_b \Lambda_{\text{QCD}}}$  serves as the renormalization point for the shape functions and the jet function. We fix this scale to  $\mu_i = 1.5 \text{ GeV}$ . Variations of  $\mu_i$  would affect both the normalization and the functional form of the shape function, as determined by the solution of the renormalization-group equation for the shape function discussed in [9, 11]. In practice, effects on the shape are irrelevant because the shape function is fitted to data. The only place where the intermediate scale has a direct impact on the extraction of  $|V_{ub}|$  is through the normalization of the shape function (45), which is multiplicative. In the analysis we therefore estimate the uncertainty by assigning the value  $\pm(\frac{\alpha_s(\mu_i)}{\pi})^2$  as a relative error. We have  $\alpha_s(\mu_i) \approx 0.354$ .
- The scale  $\bar{\mu}$  appears as the argument of  $\alpha_s$  in the perturbative contributions  $\Gamma_u^{\text{kin}}$ . We vary  $\bar{\mu}$  from  $\mu_i/\sqrt{2}$  to  $\sqrt{2}\mu_i$  with the central value  $\bar{\mu} = \mu_i = 1.5 \text{ GeV}$ .

These three errors are added in quadrature and assigned as the total perturbative uncertainty. Finally, we need to estimate the effects from higher-dimensional operators at third and higher-order in power counting. If the considered cut includes the region of phase space near the origin ( $P_+ \sim P_- \sim \Lambda_{\text{QCD}}$ ), then the dominant such contributions are weak annihilation effects, which we have discussed in Section 3.5. From the analysis in [44] one can derive a bound on the weak annihilation contribution that is  $\pm 1.8\%$  of the total decay rate, for which we take  $\Gamma_u \approx 70 |V_{ub}|^2 \text{ ps}^{-1}$  (see below). The resulting uncertainty  $\delta\Gamma_u^{\text{WA}} = \pm 1.3 |V_{ub}|^2 \text{ ps}^{-1}$  affects all partial rates which include the region near the origin in the  $(P_+, P_-)$  plane. One could avoid the uncertainty from weak annihilation by imposing a cut  $q^2 \leq q_{\text{max}}^2$  (see Section 5.6). For all observables considered in the present work, other power corrections of order  $1/m_b^3$  can be safely neglected. This can be seen by multiplying the contributions from second-order hadronic power corrections to the various decay rates (called  $\Gamma_u^{\text{hadr}(2)}$ ) by an additional suppression factor  $\Lambda_{\text{QCD}}/m_b \sim 0.2$ .

The following subsection contains a discussion of the total decay rate. In the remainder of this section we then present predictions for a variety of experimental cuts designed to eliminate (or reduce) the charm background. These partial rates can be computed either numerically or, in many cases, semi-analytically. In Appendix B we discuss how to perform the integrations over the kinematical variables  $P_l$  and  $P_-$  analytically.

## 5.1 Total decay rate

Before presenting our predictions for the various partial decay rates, it is useful to have an expression for the total  $\bar{B} \rightarrow X_u l^- \bar{\nu}$  decay rate expressed in terms of the heavy-quark parameters defined in the shape-function scheme. We start from the exact two-loop expression for the total rate derived in [51], add the second-order hadronic power corrections, which are known at tree level [12, 13], and finally convert the parameters  $m_b$  and  $\lambda_1$  from the pole scheme to

the shape-function scheme. The relevant replacements at two-loop order can be taken from [50] and read

$$\begin{aligned}
m_b^{\text{pole}} &= m_b + 0.424\mu_*\alpha_s(\mu) \left[ 1 + \left( 1.357 + 1.326 \ln \frac{\mu}{\mu_*} + 0.182 \frac{\mu_\pi^2}{\mu_*^2} \right) \alpha_s(\mu) \right] \\
&\quad + \frac{3\lambda_2 - \mu_\pi^2 - 0.330\mu_*^2\alpha_s^2(\mu)}{2m_b} + \dots, \\
-\lambda_1 &= \mu_\pi^2 + 0.330\mu_*^2\alpha_s^2(\mu) + \dots,
\end{aligned} \tag{59}$$

where  $m_b \equiv m_b(\mu_*, \mu_*)$  and  $\mu_\pi^2 \equiv \mu_\pi^2(\mu_*, \mu_*)$  are defined in the shape-function scheme. At a reference scale  $\mu_* = 1.5 \text{ GeV}$  the values of these parameters have been determined to be  $m_b = (4.61 \pm 0.08) \text{ GeV}$  and  $\mu_\pi^2 = (0.15 \pm 0.07) \text{ GeV}^2$  [50],<sup>3</sup> where we account for the small  $1/m_b$  correction to the relation for the pole mass in the above formula (corresponding to a mass shift of about  $-0.02 \text{ GeV}$  in  $m_b$ ), which was not included in that paper.

The resulting expression for the total decay rate is

$$\begin{aligned}
\Gamma_u &= \frac{G_F^2 |V_{ub}|^2 m_b^5}{192\pi^3} \left\{ 1 + \alpha_s(\mu) \left( -0.768 + 2.122 \frac{\mu_*}{m_b} \right) \right. \\
&\quad + \alpha_s^2(\mu) \left[ -2.158 + 1.019 \ln \frac{m_b}{\mu} + \left( 1.249 + 2.814 \ln \frac{\mu}{\mu_*} + 0.386 \frac{\mu_\pi^2}{\mu_*^2} \right) \frac{\mu_*}{m_b} + 0.811 \frac{\mu_*^2}{m_b^2} \right] \\
&\quad \left. - \frac{3(\mu_\pi^2 - \lambda_2)}{m_b^2} + \dots \right\}.
\end{aligned} \tag{60}$$

We observe that for  $\mu_* \approx 1.5 \text{ GeV}$  and  $\mu = O(m_b)$ , the perturbative expansion coefficients are strongly reduced compared to their values in the pole scheme ( $-0.768$  and  $-2.158$ , respectively), indicating a vastly improved convergence of the perturbative expansion. For  $m_b = \mu = 4.61 \text{ GeV}$ , and  $\mu_\pi^2 = 0.15 \text{ GeV}^2$  we obtain for the one-loop, two-loop, and power corrections inside the brackets in (60):  $\{1 - 0.017 - 0.030 - 0.004\}$ . All of these are very small corrections to the leading term.

Including the uncertainties in the values of  $m_b$  and  $\mu_\pi^2$  quoted above, and varying the renormalization scale  $\mu$  between  $m_b$  and  $m_b/2$  (with a central value of  $m_b/\sqrt{2}$ ), we get

$$\frac{\Gamma_u}{|V_{ub}|^2 \text{ ps}^{-1}} = 68.0_{-5.5}^{+5.9} [m_b] \mp 0.7 [\mu_\pi^2]_{-0.9}^{+0.6} [\mu] = (68.0 \mp 0.7 [\mu_\pi^2]_{-0.9}^{+0.6} [\mu]) \left( \frac{m_b}{4.61 \text{ GeV}} \right)^{4.81}. \tag{61}$$

Here and below, we quote values for decay rates in units of  $|V_{ub}|^2 \text{ ps}^{-1}$ . To convert these results to partial branching fractions the numbers need to be multiplied by the average  $B$ -meson lifetime. Without including the two-loop corrections, the central value in the above estimate increases to 70.6. For comparison, with the same set of input parameters our new approach based on (23) predicts a total decay rate of  $\Gamma_u = (71.2_{-5.0}^{+6.2} \pm 0.3) |V_{ub}|^2 \text{ ps}^{-1}$ , where the first error accounts for perturbative uncertainties while the second one refers to the modeling of

<sup>3</sup>The values obtained from a one-loop analysis are  $m_b = (4.55 \pm 0.08) \text{ GeV}$  and  $\mu_\pi^2 = (0.34 \pm 0.07) \text{ GeV}^2$ .

Table 1: Partial decay rate  $\Gamma_u(E_0)$  for a cut on charged-lepton energy  $E_l > E_0$  in the  $B$ -meson rest frame, given in units of  $|V_{ub}|^2 \text{ ps}^{-1}$ . Predictions are based on the shape-function parameter values  $m_b = 4.61 \text{ GeV}$ ,  $\mu_\pi^2 = 0.2 \text{ GeV}^2$  (top) and  $m_b = 4.55 \text{ GeV}$ ,  $\mu_\pi^2 = 0.3 \text{ GeV}^2$  (bottom).

$E_0$ [GeV]	Mean	Subl. SF	Pert.	Total
1.9	24.39	$\pm 0.35$	+1.85 -1.61	+2.27 -2.08
2.0	18.64	$\pm 0.44$	+1.32 -1.17	+1.88 -1.77
2.1	13.00	$\pm 0.59$	+0.82 -0.75	+1.62 -1.58
2.2	7.82	$\pm 0.80$	+0.42 -0.39	+1.55 -1.55
2.3	3.64	$\pm 0.96$	+0.15 -0.14	+1.59 -1.59
2.4	1.00	$\pm 0.82$	+0.04 -0.03	+1.51 -1.51
1.9	19.32	$\pm 0.62$	+1.41 -1.17	+1.99 -1.83
2.0	14.30	$\pm 0.77$	+0.96 -0.79	+1.76 -1.67
2.1	9.58	$\pm 0.96$	+0.58 -0.47	+1.69 -1.65
2.2	5.46	$\pm 1.17$	+0.31 -0.22	+1.75 -1.74
2.3	2.33	$\pm 1.26$	+0.14 -0.13	+1.78 -1.78
2.4	0.46	$\pm 1.01$	+0.05 -0.08	+1.61 -1.61

subleading shape functions (to which there is essentially no sensitivity at all in the total rate). The fact that this is in excellent agreement with the direct calculation using (60) supports the notion that the formalism developed in this work can be used to describe arbitrary  $\bar{B} \rightarrow X_u l^- \bar{\nu}$  decay distributions, both in the shape-function region and in the OPE region of phase space.

## 5.2 Cut on charged-lepton energy

Traditionally, the most common variable to discriminate against the charm background is the charged-lepton energy  $E_l$ . As long as one requires that  $E_l$  is bigger than  $(M_B^2 - M_D^2)/2M_B \approx 2.31 \text{ GeV}$ , the final hadronic state cannot have an invariant mass larger than  $M_D$ . For this ideal cut with the default set of subleading shape functions (51)

$$\begin{aligned} & \Gamma_u^{(0)} + (\Gamma_u^{\text{kin}(1)} + \Gamma_u^{\text{hadr}(1)}) + (\Gamma_u^{\text{kin}(2)} + \Gamma_u^{\text{hadr}(2)}) \\ &= [6.810 + (0.444 - 2.851) + (0.042 - 0.649)] |V_{ub}|^2 \text{ ps}^{-1}. \end{aligned} \quad (62)$$

The corrections from subleading shape functions are quite sizable, in accordance with the findings in [28, 29, 30]. Note that the sum  $\Gamma_u^{\text{kin}(1)} + \Gamma_u^{\text{kin}(2)} = 0.486$  is an excellent approximation to the exact result  $\Gamma_u^{\text{kin}} = 0.482$  (all in units of  $|V_{ub}|^2 \text{ ps}^{-1}$ ) obtained using (30), indicating that the Taylor expansion of the kinematical power corrections is converging rapidly. The same will be true for all other observables considered below.

In practice, the cut can be relaxed to some extent, because the background is well understood, thereby increasing the efficiency and reducing the impact of theoretical uncertainties.

Table 2: Same as Table 1, but for the partial decay rate  $\gamma \Gamma_u(E_0)$  for a cut on lepton energy  $E_l > E_0$  in the  $\Upsilon(4S)$  rest frame.

$E_0$ [GeV]	Mean	Subl. SF	Pert.	Total
1.9	24.43	$\pm 0.36$	+1.86 -1.62	+2.28 -2.08
2.0	18.74	$\pm 0.45$	+1.34 -1.18	+1.89 -1.79
2.1	13.21	$\pm 0.61$	+0.86 -0.77	+1.64 -1.60
2.2	8.22	$\pm 0.79$	+0.47 -0.43	+1.56 -1.55
2.3	4.26	$\pm 0.85$	+0.21 -0.20	+1.54 -1.53
2.4	1.69	$\pm 0.63$	+0.07 -0.07	+1.41 -1.41
1.9	19.40	$\pm 0.64$	+1.43 -1.18	+2.01 -1.84
2.0	14.45	$\pm 0.78$	+0.98 -0.81	+1.78 -1.69
2.1	9.82	$\pm 0.97$	+0.61 -0.49	+1.70 -1.66
2.2	5.84	$\pm 1.13$	+0.34 -0.25	+1.73 -1.71
2.3	2.84	$\pm 1.13$	+0.17 -0.13	+1.70 -1.70
2.4	0.98	$\pm 0.84$	+0.07 -0.07	+1.51 -1.51

Our findings for different values of the cut  $E_0$  are summarized in Table 1. Here and below, the columns have the following meaning: “Mean” denotes the prediction for the partial decay rate  $\Gamma_u$ , “Subl. SF” the uncertainty from subleading shape functions, “Pert.” the total perturbative uncertainty, and in the column “Total” we added the stated errors plus the uncertainty from weak annihilation in quadrature.

Experiments often do not measure the partial rates in the  $B$ -meson rest frame, but work at the  $\Upsilon(4S)$  resonance. Boosting to the  $\Upsilon(4S)$  frame with  $\beta = v/c \approx 0.064$  has a small effect on the spectrum and rates. The exact formula for this boost is

$$\gamma \Gamma_u^{(\Upsilon)}(E_0) = \frac{1}{\beta_+ - \beta_-} \int_{\beta_- E_0}^{M_B/2} dE \frac{d\Gamma_u^{(B)}}{dE} \left[ \beta_+ - \max\left(\beta_-, \frac{E_0}{E}\right) \right], \quad (63)$$

where  $\beta_{\pm} = \sqrt{1 \pm \beta}/\sqrt{1 \mp \beta}$ , and the factor  $\gamma = 1/\sqrt{1 - \beta^2} \approx 1.002$  on the left-hand side takes the time dilation of the  $B$ -meson lifetime  $\tau'_B = \gamma \tau_B$  into account. (In other words, branching fractions are Lorentz invariant.) The above formula can be accurately approximated by the first term in an expansion in  $\beta^2$ , which yields [24]

$$\gamma \Gamma_u^{(\Upsilon)}(E_0) = \Gamma_u^{(B)}(E_0) - \frac{\beta^2}{6} E_0^3 \left[ \frac{d}{dE} \frac{1}{E} \frac{d\Gamma_u^{(B)}}{dE} \right]_{E=E_0} + O(\beta^4), \quad (64)$$

as long as  $E_0$  is not too close to the kinematical endpoint (i.e.,  $E_0 \leq \beta_- M_B/2 \approx 2.47$  GeV). The numerical results for the partial decay rate  $\gamma \Gamma_u^{(\Upsilon)}(E_0)$  in the rest frame of the  $\Upsilon(4S)$  resonance are given in Table 2.

### 5.3 Cut on hadronic $P_+$

Cutting on  $P_+$  samples the same hadronic phase space as a cut on the charged-lepton energy, but with much better efficiency [9, 14]. The phase space  $P_+ \leq \Delta_P$  with the ideal separator  $\Delta_P = M_D^2/M_B \approx 0.66$  GeV contains well over half of all  $\bar{B} \rightarrow X_u l^- \bar{\nu}$  events. Here we find with the default settings

$$\begin{aligned} & \Gamma_u^{(0)} + (\Gamma_u^{\text{kin}(1)} + \Gamma_u^{\text{hadr}(1)}) + (\Gamma_u^{\text{kin}(2)} + \Gamma_u^{\text{hadr}(2)}) \\ &= [53.225 + (4.646 - 11.746) + (0.328 - 0.469)] |V_{ub}|^2 \text{ps}^{-1}. \end{aligned} \quad (65)$$

We see a much better convergence of the power series than in the case of a cut on the charged-lepton energy endpoint, namely  $53.225 - 7.100 - 0.141$  when grouping the above numbers according to their power counting. Once again, the sum  $\Gamma_u^{\text{kin}(1)} + \Gamma_u^{\text{kin}(2)} = 4.974$  is very close to the full kinematical correction  $\Gamma_u^{\text{kin}} = 4.959$  (in units of  $|V_{ub}|^2 \text{ps}^{-1}$ ).

Often times it is required to impose an additional cut on the charged-lepton energy, as leptons that are too soft are difficult to detect. In Table 3 we list results for both  $E_l \geq 0$  and  $E_l \geq 1.0$  GeV. For the ideal cut we find that the prediction is quite precise, as the theoretical uncertainty is about 6.6%. For comparison, the ideal cut for the lepton energy is uncertain by about 40%, but rapidly improving as the energy cut is relaxed.

### 5.4 Cut on hadronic in variant mass and $q^2$

The most efficient separator for the discrimination of charmed events is a cut on the invariant mass  $M_X$  of the final hadronic state  $M_X \leq M_D$  [52, 53]. It has also been argued [54, 55] that a cut on  $q^2$  can reduce the shape-function sensitivity, since the large  $P_-$  region is avoided and the  $P_+$  integration domain is rather large. In order to optimize signal efficiency and theoretical uncertainties, a  $q^2$  cut is often combined with a cut on hadronic invariant mass. In Table 4 we give results for typical cuts on both variables, with and without including an additional cut on charged-lepton energy.

Let us study the contributions for a the optimal cut  $M_X \leq M_D$  in detail. We find with the default settings

$$\begin{aligned} & \Gamma_u^{(0)} + (\Gamma_u^{\text{kin}(1)} + \Gamma_u^{\text{hadr}(1)}) + (\Gamma_u^{\text{kin}(2)} + \Gamma_u^{\text{hadr}(2)}) \\ &= [58.541 + (8.027 - 9.742) + (2.100 - 0.661)] |V_{ub}|^2 \text{ps}^{-1}. \end{aligned} \quad (66)$$

Note the almost perfect (accidental) cancellation of the two terms at order  $1/m_b$ . The resulting power series,  $58.541 - 1.715 + 1.439$ , again exhibits good convergence. As previously, the sum  $\Gamma_u^{\text{kin}(1)} + \Gamma_u^{\text{kin}(2)} = 10.127$  is a good approximation to the exact value  $\Gamma_u^{\text{kin}} = 9.753$  (in units of  $|V_{ub}|^2 \text{ps}^{-1}$ ). The analogous analysis for a combined cut  $M_X \leq 1.7$  GeV and  $q^2 \geq 8.0$  GeV<sup>2</sup> reads

$$\begin{aligned} & \Gamma_u^{(0)} + (\Gamma_u^{\text{kin}(1)} + \Gamma_u^{\text{hadr}(1)}) + (\Gamma_u^{\text{kin}(2)} + \Gamma_u^{\text{hadr}(2)}) \\ &= [25.880 + (4.049 - 6.625) + (1.399 - 0.370)] |V_{ub}|^2 \text{ps}^{-1}, \end{aligned} \quad (67)$$

which means that the power series is  $25.880 - 2.576 + 1.029$ . Here we have  $\Gamma_u^{\text{kin}(1)} + \Gamma_u^{\text{kin}(2)} = 5.448$ , which is close to  $\Gamma_u^{\text{kin}} = 5.160$  (in units of  $|V_{ub}|^2 \text{ps}^{-1}$ ).

Table 3: Partial decay rate  $\Gamma_u(\Delta_P, E_0)$  for a cut on the hadronic variable  $P_+ \leq \Delta_P$  and lepton energy  $E_l \geq E_0$ , given in units of  $|V_{ub}|^2 \text{ps}^{-1}$ . Predictions are based on the shape-function parameter values  $m_b = 4.61 \text{ GeV}$ ,  $\mu_\pi^2 = 0.2 \text{ GeV}^2$  (top) and  $m_b = 4.55 \text{ GeV}$ ,  $\mu_\pi^2 = 0.3 \text{ GeV}^2$  (bottom).

$\Delta_P$ [GeV]	$E_0$ [GeV]	Mean	Subl. SF	Pert.	Total
0.70	0.0	48.48	$\pm 0.74$	+2.82 -2.65	+3.17 -3.02
0.65	0.0	45.14	$\pm 0.98$	+2.59 -2.45	+3.04 -2.92
0.60	0.0	41.39	$\pm 1.22$	+2.35 -2.24	+2.93 -2.84
0.55	0.0	37.21	$\pm 1.46$	+2.11 -2.01	+2.86 -2.78
0.50	0.0	32.62	$\pm 1.65$	+1.86 -1.77	+2.79 -2.73
0.70	1.0	42.92	$\pm 0.69$	+2.53 -2.38	+2.91 -2.78
0.65	1.0	39.96	$\pm 0.92$	+2.33 -2.21	+2.80 -2.70
0.60	1.0	36.62	$\pm 1.17$	+2.12 -2.02	+2.73 -2.65
0.55	1.0	32.90	$\pm 1.41$	+1.90 -1.82	+2.68 -2.62
0.50	1.0	28.82	$\pm 1.62$	+1.68 -1.60	+2.65 -2.60
0.70	0.0	37.81	$\pm 1.26$	+2.05 -1.94	+2.71 -2.63
0.65	0.0	35.03	$\pm 1.49$	+1.86 -1.78	+2.69 -2.64
0.60	0.0	32.01	$\pm 1.71$	+1.67 -1.63	+2.70 -2.68
0.55	0.0	28.74	$\pm 1.90$	+1.49 -1.47	+2.73 -2.71
0.50	0.0	25.24	$\pm 2.04$	+1.32 -1.30	+2.74 -2.73
0.70	1.0	33.31	$\pm 1.22$	+1.83 -1.73	+2.53 -2.46
0.65	1.0	30.86	$\pm 1.45$	+1.66 -1.59	+2.54 -2.50
0.60	1.0	28.18	$\pm 1.68$	+1.49 -1.45	+2.58 -2.55
0.55	1.0	25.29	$\pm 1.88$	+1.33 -1.31	+2.63 -2.62
0.50	1.0	22.18	$\pm 2.03$	+1.18 -1.17	+2.67 -2.66

Table 4: Partial decay rate  $\Gamma_u(M_0, q_0^2, E_0)$  for combined hadronic cuts  $M_X \leq M_0$ ,  $q^2 > q_0^2$ , and lepton energy  $E_l \geq E_0$ , given in units of  $|V_{ub}|^2 \text{ps}^{-1}$ . Predictions are based on the shape-function parameter values  $m_b = 4.61 \text{ GeV}$ ,  $\mu_\pi^2 = 0.2 \text{ GeV}^2$  (top) and  $m_b = 4.55 \text{ GeV}$ ,  $\mu_\pi^2 = 0.3 \text{ GeV}^2$  (bottom).

$M_0$ [GeV]	$q_0^2$ [GeV <sup>2</sup> ]	$E_0$ [GeV]	Mean	Subl. SF	Pert.	Total
$M_D$	0.0	0.0	58.27	$\pm 0.25$	+4.12 -3.64	+4.31 -3.86
1.70	0.0	0.0	51.95	$\pm 0.60$	+3.55 -3.20	+3.81 -3.49
1.55	0.0	0.0	44.59	$\pm 0.90$	+2.99 -2.74	+3.37 -3.15
$M_D$	6.0	0.0	33.76	$\pm 0.21$	+2.90 -2.51	+3.17 -2.82
1.70	8.0	0.0	24.31	$\pm 0.23$	+2.17 -1.91	+2.52 -2.30
$M_D$	$(M_B - M_D)^2$	0.0	12.39	$\pm 0.40$	+1.39 -1.22	+1.92 -1.80
$M_D$	0.0	1.0	52.52	$\pm 0.13$	+3.82 -3.36	+4.02 -3.59
1.70	0.0	1.0	47.21	$\pm 0.40$	+3.31 -2.98	+3.57 -3.26
1.55	0.0	1.0	40.88	$\pm 0.67$	+2.80 -2.56	+3.15 -2.93
$M_D$	6.0	1.0	33.27	$\pm 0.21$	+2.86 -2.48	+3.14 -2.79
1.70	8.0	1.0	24.25	$\pm 0.23$	+2.17 -1.91	+2.52 -2.30
$M_D$	$(M_B - M_D)^2$	1.0	12.39	$\pm 0.40$	+1.39 -1.22	+1.92 -1.80
$M_D$	0.0	0.0	47.42	$\pm 0.28$	+3.26 -2.85	+3.50 -3.13
1.70	0.0	0.0	41.60	$\pm 0.50$	+2.70 -2.42	+3.02 -2.78
1.55	0.0	0.0	35.37	$\pm 0.68$	+2.19 -2.01	+2.62 -2.47
$M_D$	6.0	0.0	27.32	$\pm 0.40$	+2.29 -1.94	+2.65 -2.35
1.70	8.0	0.0	19.02	$\pm 0.51$	+1.64 -1.41	+2.13 -1.96
$M_D$	$(M_B - M_D)^2$	0.0	9.31	$\pm 0.65$	+1.04 -0.87	+1.76 -1.66
$M_D$	0.0	1.0	42.68	$\pm 0.27$	+3.02 -2.63	+3.28 -2.92
1.70	0.0	1.0	37.70	$\pm 0.44$	+2.52 -2.25	+2.85 -2.61
1.55	0.0	1.0	32.21	$\pm 0.68$	+2.05 -1.88	+2.50 -2.36
$M_D$	6.0	1.0	26.89	$\pm 0.40$	+2.26 -1.91	+2.62 -2.33
1.70	8.0	1.0	18.97	$\pm 0.51$	+1.64 -1.40	+2.13 -1.95
$M_D$	$(M_B - M_D)^2$	1.0	9.31	$\pm 0.65$	+1.04 -0.87	+1.76 -1.66

Table 5: Partial decay rate  $\Gamma_u(s_0, E_0)$  for combined cuts  $s_H^{\max} \leq s_0$  and lepton energy  $E_l \geq E_0$ , given in units of  $|V_{ub}|^2 \text{ps}^{-1}$ . Predictions are based on the shape-function parameter values  $m_b = 4.61 \text{ GeV}$ ,  $\mu_\pi^2 = 0.2 \text{ GeV}^2$  (top) and  $m_b = 4.55 \text{ GeV}$ ,  $\mu_\pi^2 = 0.3 \text{ GeV}^2$  (bottom).

$s_0$ [GeV <sup>2</sup> ]	$E_0$ [GeV]	Mean	Subl. SF	Pert.	Total
3.5	1.8	17.18	$\pm 0.47$	+1.51	+2.02
				-1.33	-1.89
3.5	1.9	15.65	$\pm 0.49$	+1.30	+1.87
				-1.15	-1.77
3.5	2.0	13.55	$\pm 0.53$	+1.03	+1.71
				-0.92	-1.65
3.5	2.1	10.77	$\pm 0.64$	+0.71	+1.58
				-0.65	-1.55
3.5	1.8	13.09	$\pm 0.77$	+1.11	+1.84
				-0.93	-1.74
3.5	1.9	11.74	$\pm 0.80$	+0.93	+1.76
				-0.77	-1.68
3.5	2.0	9.95	$\pm 0.87$	+0.72	+1.69
				-0.59	-1.64
3.5	2.1	7.70	$\pm 1.01$	+0.50	+1.69
				-0.39	-1.66

## 5.5 Cut on $s_H^{\max}$ and $E_l$

In [56] the BaBar collaboration employed a cut on both  $E_l \geq E_0$  and a new kinematical variable  $s_H^{\max} \leq s_0$ , where the definition for  $s_H^{\max}$  involves both hadronic and leptonic variables. In the  $B$ -meson rest frame it is

$$s_H^{\max} = M_B^2 + q^2 - 2M_B \left( E_l + \frac{q^2}{4E_l} \right). \quad (68)$$

Rewriting the phase space of this cut in the variables  $P_+$ ,  $P_-$ ,  $P_l$ , we find

$$\begin{aligned} 0 &\leq P_+ \leq \min(M_B - 2E_0, \sqrt{s_0}), \\ P_+ &\leq P_- \leq \min\left(\frac{s_0}{P_+}, M_B\right), \\ P_+ &\leq P_l \leq \min(M_B - 2E_0, P_-), \end{aligned} \quad (69)$$

where it is understood that if  $q^2 = (M_B - P_+)(M_B - P_-) \leq (M_B - \sqrt{s_0})^2$ , then the interval  $P_l^{\min} < P_l < P_l^{\max}$  must be *excluded* from the  $P_l$  integration. Here

$$P_l^{\max/\min}(P_+, P_-) = \left( \frac{P_+ + P_-}{2} + \frac{s_0 - P_+ P_-}{2M_B} \right) \pm \sqrt{\left( \frac{P_+ + P_-}{2} + \frac{s_0 - P_+ P_-}{2M_B} \right)^2 - s_0}. \quad (70)$$

A summary of our findings is given in Table 5. When compared to the pure charged-lepton energy cut in Table 1, the additional cut on  $s_H^{\max}$  eliminates roughly another 20–30% of events. However, the hope is that this cut also reduces the sensitivity to the leading shape function, which we expect to be sizable for the pure  $E_l$  cut. The uncertainty from subleading shape functions, however, is almost unaffected by the  $s_H^{\max}$  cut.

Table 6: Examples for partial decay rates with cuts on  $q^2 \leq (M_B - M_D)^2$ . We consider an additional cut on the hadronic variable  $P_+ \leq \Delta_P$  (top), or on the hadronic mass  $M_X \leq M_0$  (bottom). As before, decay rates are given in units of  $|V_{ub}|^2 \text{ps}^{-1}$ . Predictions are based on the shape-function parameters  $m_b = 4.61 \text{ GeV}$  and  $\mu_\pi^2 = 0.2 \text{ GeV}^2$ .

$\Delta_P$ [GeV]	Mean	Subl. SF	Pert.	Total
0.70	39.24	$\pm 0.88$	+2.10 -1.96	+2.28 -2.14
0.65	36.51	$\pm 1.04$	+1.94 -1.81	+2.20 -2.09
0.60	33.46	$\pm 1.20$	+1.77 -1.66	+2.14 -2.05
0.55	30.07	$\pm 1.33$	+1.59 -1.49	+2.08 -2.00
0.50	26.39	$\pm 1.40$	+1.41 -1.31	+1.98 -1.91
$M_0$ [GeV]	Mean	Subl. SF	Pert.	Total
$M_D$	45.79	$\pm 0.56$	+2.73 -2.43	+2.79 -2.49
1.70	39.56	$\pm 0.86$	+2.22 -2.03	+2.38 -2.20
1.55	32.63	$\pm 1.15$	+1.79 -1.65	+2.13 -2.02

## 5.6 Eliminating weak annihilation contributions

In Section 3.5 we have argued that a cut on *high*  $q^2$ , i.e.,  $q^2 < q_0^2$ , will eliminate the effect of weak annihilation and remove the uncertainty associated with this contribution. The cutoff  $q_0^2$  should be small enough to exclude the region around  $q^2 = m_b^2$ , where this contribution is concentrated. It is instructive to assess the “cost” of such an additional cut in terms of the loss of efficiency and, more importantly, the behavior of the remaining uncertainties. We investigate the effect using the generous cut  $q_0^2 = (M_B - M_D)^2$ , and combine it with two other typical cuts which discriminate against charm background:  $M_X$  or  $P_+$ . While this particular choice for  $q_0^2$  still leaves some room to improve the efficiency by increasing  $q_0^2$ , it is not desirable to raise the cut much further, since this would threaten the validity of quark-hadron duality.

The results are summarized in Table 6 and can be compared to the previous “pure”  $P_+$  and  $M_X$  cuts in Tables 3 and 4. As an example, let us consider the case  $P_+ \leq 0.65 \text{ GeV}$ , which is close to the charm threshold. Without the additional  $q^2$  cut we found that the total theoretical uncertainty (including the weak annihilation error) is  ${}^{+6.7\%}_{-6.5\%}$ . When cutting in addition on  $q^2 \leq (M_B - M_D)^2$ , the efficiency decreases by about 20% as expected. However, due to the absence of the weak annihilation uncertainty, the overall uncertainty decreases to  ${}^{+6.0\%}_{-5.7\%}$ . Therefore both strategies result in comparable relative uncertainties, with a slight favor for imposing the additional cut from the theoretical point of view.

While the small reduction of theoretical errors hardly seems worth the effort of imposing the  $q^2$  cut, performing an analysis of the type outlined here and comparing its results with those obtained without the additional cut may help to corroborate that the weak annihilation contribution is indeed not much larger than what has been found in [44].

Table 7: Values of the exponent  $a(m_b)$  for different kinematical cuts. The parameter  $\mu_\pi^2 = 0.2 \text{ GeV}^2$  is kept fixed. Also quoted is the sensitivity of the partial decay rates to the functional form of the shape functions. See text for explanation.

	$m_b$ [GeV]	4.50	4.55	4.60	4.65	4.70
$M_X \leq M_D$	$a$	9.8	9.1	8.4	7.9	7.4
	Functional Form	1.0%	1.2%	1.5%	2.0%	2.7%
$M_X \leq 1.7 \text{ GeV}$	$a$	12.8	11.7	10.7	9.9	9.1
	Functional Form	2.0%	2.3%	2.7%	3.2%	3.9%
$M_X \leq 1.7 \text{ GeV}$ $q^2 \geq 8 \text{ GeV}^2$	$a$	10.6	10.0	9.6	9.2	8.9
	Functional Form	2.4%	2.0%	1.6%	1.1%	0.9%
$q^2 \geq (M_B - M_D)^2$	$a$	11.9	11.6	11.3	11.1	10.9
	Functional Form	5.2%	4.6%	4.0%	3.4%	2.9%
$P_+ \leq M_D^2/M_B$	$a$	16.5	14.7	13.2	11.9	10.7
	Functional Form	5.2%	5.0%	4.9%	4.8%	5.1%
$E_l \geq 2.2 \text{ GeV}$	$a$	21.0	19.7	18.5	17.5	16.6
	Functional Form	16.5%	13.4%	10.9%	9.0%	7.7%

## 5.7 Dependence on $m_b$ and shape-function sensitivity

Non-perturbative hadronic physics enters in our approach via the form of the leading and subleading shape functions. The strongest sensitivity by far is to the first moment of the leading shape function, which determines the HQET parameter  $\bar{\Lambda}$  and with it the  $b$ -quark mass. Given that the value of  $m_b \equiv m_b(\mu_*, \mu_*)$  can be determined with good precision from other sources (such as moments of the lepton or hadronic invariant mass spectra in  $\bar{B} \rightarrow X_c l \bar{\nu}$  decays), it is instructive to disentangle this dependence from the sensitivity to higher moments or, more generally, to the functional form of the shape functions for fixed  $m_b$ .

To explore the dependence on  $m_b$  we define the exponent

$$a(m_b) = \frac{d \ln \Gamma_u}{d \ln m_b} = \left( \frac{\Delta \Gamma_u}{\Gamma_u} \right) / \left( \frac{\Delta m_b}{m_b} \right), \quad (71)$$

which means that  $\Gamma_u \sim (m_b)^a$ . Table 7 shows the values of this exponent over a wide range of values of  $m_b$  for a variety of experimental cuts. To estimate the sensitivity to the functional form we scan over the six models for the subleading shape functions, and we also study the difference between the results obtained using the exponential or the gaussian ansatz for the leading shape function. The corresponding variations are added in quadrature and given as a relative change in the corresponding partial decay rates (labeled ‘‘Functional Form’’). In all cases,  $\mu_\pi^2 = 0.2 \text{ GeV}^2$  is kept fixed.

The entries in the table are listed in roughly the order of increasing sensitivity to  $m_b$  and to the functional form of the shape functions, with the hadronic invariant mass cut showing

the least sensitivity and the lepton energy cut exhibiting the largest one. To some extent this reflects the different efficiencies (or “inclusiveness”) of the various cuts. It is reassuring that  $a \approx 10$  for the pure  $q^2$  cut, in accordance with the findings of [38, 39]. Perhaps somewhat surprisingly, for this cut a substantial sensitivity to shape-function effects remains even for fixed  $m_b$  and  $\mu_\pi^2$ . It is well known that the partial rate with a cut  $q^2 \geq (M_B - M_D)^2$  can be calculated using a local OPE in powers of  $\Lambda_{\text{QCD}}/m_c$  [38, 54], thereby avoiding the notion of shape-function sensitivity. Differences between the functional forms of the shape functions in our approach correspond to effects that are formally of order  $1/m_c^3$  and higher. It is not unreasonable that these effects should be of order 3–5%.

We also checked that for much more relaxed cuts the value of  $a(m_b)$  tends to 4.8, as stated in (61). For example, for a cut  $P_+ \leq \Delta_P$  we find (with  $m_b = 4.61 \text{ GeV}$  and  $\mu_\pi^2 = 0.2 \text{ GeV}^2$ ):

$\Delta_P$ [GeV]	0.6	0.8	1.0	1.2	1.4
$a$	14.9	9.6	7.1	6.0	5.5
Functional Form	5.9%	2.4%	0.3%	0.5%	0.4%

## 6 Conclusions

A high-precision measurement of the parameters of the unitarity triangle is an ongoing quest, which necessitates the close cooperation of theory and experiment. The determination of  $|V_{ub}|$  from inclusive  $\bar{B} \rightarrow X_u l^- \bar{\nu}$  decay requires the measurement of partial decay rates with kinematical cuts that eliminate the large background from  $\bar{B} \rightarrow X_c l^- \bar{\nu}$  decays, as well as theoretical predictions for such quantities. To this end, it is desirable to have a theoretical description of the triple differential decay rate, which can be used for predicting arbitrary partial rates obtained after integrating over certain regions of phase space. One problem in providing such a description is that the power-counting rules of the heavy-quark expansion are different in different kinematical domains. In this paper we have overcome this difficulty.

In the shape-function region, our results are in agreement with QCD factorization theorems, and perturbative effects have been separated from non-perturbative shape functions. When the allowed phase space extends over a large domain, our results smoothly reduce to the expressions obtained from the local operator product expansion. We have presented a formalism in which event distributions and partial decay rates are expressed without explicit reference to partonic quantities such as the  $b$ -quark mass. The sensitivity to such hadronic parameters enters indirectly, via the moments of shape functions. The most important non-perturbative object, namely the leading-order shape function, can be extracted from the photon spectrum in  $\bar{B} \rightarrow X_s \gamma$  decays, for which we have presented a detailed description analogous to our treatment of  $\bar{B} \rightarrow X_u l^- \bar{\nu}$  event distributions. This is analogous to extractions of parton distribution functions from fits to data on deep inelastic scattering. In this way, the dominant uncertainty from our ignorance about bound-state effects in the  $B$  meson is turned into an experimental uncertainty, which will reduce with increasing accuracy of the experimental data on the photon spectrum. Residual hadronic uncertainties are power suppressed in the heavy-quark expansion.

One goal of this paper was to present a detailed framework in which this program can be carried out. We have given formulae that can be readily used for the construction of an

event generator, as well as to estimate the remaining theoretical uncertainties in a robust and automated fashion.

In practice the leading shape function needs to be parameterized. We have suggested three different functional forms, which can be used to fit the data of the  $\bar{B} \rightarrow X_s \gamma$  photon spectrum. Once the data is accurately described by a set of shape functions, this set can be used in the predictions for partial  $\bar{B} \rightarrow X_u l^- \bar{\nu}$  rates and spectra. The subleading shape functions, which come in a different linear combination than in the  $\bar{B} \rightarrow X_s \gamma$  case, give rise to theoretical uncertainties starting at the level of  $1/m_b$  power corrections. We have estimated these uncertainties using a set of models, each of which obeys the known tree-level moment relations, but which are very different in their functional form. A second error estimate is determined by the residual renormalization-scale dependence. We also considered uncertainties from weak annihilation effects, which can be avoided by cutting away the region of phase space in which they contribute. We have suggested a cut on high lepton invariant mass, which accomplishes just that.

Numerical predictions and the theoretical errors have been assembled in the second half of this paper. We have presented results for many experimental cuts, including cuts on the charged-lepton energy (both in the rest frame of the  $B$ -meson and the  $\Upsilon(4S)$  resonance), on the hadronic  $P_+$  variable, on  $M_X$ , on  $q^2$ , and on various combinations of these cuts. Once the data on the  $\bar{B} \rightarrow X_s \gamma$  photon spectrum are sufficiently precise to accurately determine the leading-order shape function, a determination of  $|V_{ub}|$  seems feasible with theory uncertainties at the 5–10% level.

*Acknowledgments:* We are grateful to many of our colleagues in both experiment and theory. We thank Christian Bauer, Ilija Bizjak, Riccardo Faccini, Lawrence Gibbons, Vladimir Golubev, Robert Kowalewski, Seung Lee, Zoltan Ligeti, Antonio Limosani, Francesca Di Lodovico, Vera Luth, Thomas Meyer, Masahiro Morii, Franz Muheim, and Tadao Nozaki for valuable discussions. We would like to thank the Institute for Advanced Study, Princeton, NJ, where part of this work was done, for their hospitality. The work of B.O.L. was supported in part by funds provided by the U.S. Department of Energy (D.O.E.) under cooperative research agreement DE-FC02-94ER40818. The research of M.N. and G.P. was supported by the National Science Foundation under Grant PHY-0355005.

# A Perturbative Expressions

## A.1 Anomalous dimensions

Here we list the known perturbative expansions of the  $\beta$ -function and relevant anomalous dimensions. We work in the  $\overline{\text{MS}}$  scheme and define

$$\beta(\alpha_s) = \frac{d\alpha_s(\mu)}{d\ln\mu} = -2\alpha_s \sum_{n=0}^{\infty} \beta_n \left(\frac{\alpha_s}{4\pi}\right)^{n+1},$$

$$\Gamma_{\text{cusp}}(\alpha_s) = \sum_{n=0}^{\infty} \Gamma_n \left(\frac{\alpha_s}{4\pi}\right)^{n+1}, \quad \gamma'(\alpha_s) = \sum_{n=0}^{\infty} \gamma'_n \left(\frac{\alpha_s}{4\pi}\right)^{n+1}, \quad (72)$$

as the expansion coefficients for the  $\beta$ -function, the leading order SCET current anomalous dimension, and the cusp anomalous dimension. To three-loop order, the  $\beta$  function reads [57]

$$\beta_0 = \frac{11}{3} C_A - \frac{2}{3} n_f, \quad \beta_1 = \frac{34}{3} C_A^2 - \frac{10}{3} C_A n_f - 2C_F n_f,$$

$$\beta_2 = \frac{2857}{54} C_A^3 + \left(C_F^2 - \frac{205}{18} C_F C_A - \frac{1415}{54} C_A^2\right) n_f + \left(\frac{11}{9} C_F + \frac{79}{54} C_A\right) n_f^2, \quad (73)$$

where  $n_f = 4$  is the number of light flavors,  $C_A = 3$  and  $C_F = 4/3$ . The three-loop expression for the cusp anomalous dimension has recently been obtained in [58]. The coefficients read

$$\Gamma_0 = 4C_F, \quad \Gamma_1 = 8C_F \left[ \left(\frac{67}{18} - \frac{\pi^2}{6}\right) C_A - \frac{5}{9} n_f \right],$$

$$\Gamma_2 = 16C_F \left[ \left(\frac{245}{24} - \frac{67\pi^2}{54} + \frac{11\pi^4}{180} + \frac{11}{6} \zeta_3\right) C_A^2 + \left(-\frac{209}{108} + \frac{5\pi^2}{27} - \frac{7}{3} \zeta_3\right) C_A n_f \right. \\ \left. + \left(-\frac{55}{24} + 2\zeta_3\right) C_F n_f - \frac{1}{27} n_f^2 \right]. \quad (74)$$

The SCET anomalous dimension  $\gamma$  is explicitly known only to one-loop order. However, the two-loop coefficient can be extracted by noting that  $\gamma$  is related to the axial-gauge anomalous dimension in deep-inelastic scattering [11]. The result is

$$\gamma'_0 = -5C_F, \quad (75)$$

$$\gamma'_1 = -8C_F \left[ \left(\frac{3}{16} - \frac{\pi^2}{4} + 3\zeta_3\right) C_F + \left(\frac{1549}{432} + \frac{7\pi^2}{48} - \frac{11}{4} \zeta_3\right) C_A - \left(\frac{125}{216} + \frac{\pi^2}{24}\right) n_f \right].$$

## A.2 Sudakov factor

The exact expression for the Sudakov factor reads

$$\ln U(\mu_h, \mu_i) = 2S_\Gamma(\mu_h, \mu_i) - 2a_\Gamma(\mu_h, \mu_i) \ln \frac{m_b}{\mu_h} - 2a_{\gamma'}(\mu_h, \mu_i), \quad (76)$$

where the functions of the right-hand side are solutions to the renormalization-group equations

$$\begin{aligned} \frac{d}{d \ln \mu} S_\Gamma(\nu, \mu) &= -\Gamma_{\text{cusp}}(\alpha_s(\mu)) \ln \frac{\mu}{\nu}, \\ \frac{d}{d \ln \mu} a_\Gamma(\nu, \mu) &= -\Gamma_{\text{cusp}}(\alpha_s(\mu)), \quad \frac{d}{d \ln \mu} a_{\gamma'}(\nu, \mu) = -\gamma'(\alpha_s(\mu)), \end{aligned} \quad (77)$$

with boundary conditions  $S(\nu, \mu) = 0$  etc. at  $\mu = \nu$ . These equations can be integrated using that  $d/d \ln \mu = \beta(\alpha_s) d/d\alpha_s$ . The solutions are

$$S_\Gamma(\nu, \mu) = - \int_{\alpha_s(\nu)}^{\alpha_s(\mu)} d\alpha \frac{\Gamma_{\text{cusp}}(\alpha)}{\beta(\alpha)} \int_{\alpha_s(\nu)}^{\alpha} \frac{d\alpha'}{\beta(\alpha')}, \quad a_\Gamma(\nu, \mu) = - \int_{\alpha_s(\nu)}^{\alpha_s(\mu)} d\alpha \frac{\Gamma_{\text{cusp}}(\alpha)}{\beta(\alpha)}, \quad (78)$$

and similarly for  $a_{\gamma'}$ .

Next, we give explicit results for the Sudakov function  $S_\Gamma$  and the functions  $a_\Gamma$  and  $a_\gamma$  in (76) at next-to-leading order in renormalization-group improved perturbation theory. We obtain

$$a_\Gamma(\nu, \mu) = \frac{\Gamma_0}{2\beta_0} \left[ \ln \frac{\alpha_s(\mu)}{\alpha_s(\nu)} + \left( \frac{\Gamma_1}{\Gamma_0} - \frac{\beta_1}{\beta_0} \right) \frac{\alpha_s(\mu) - \alpha_s(\nu)}{4\pi} + \dots \right], \quad (79)$$

and similarly for  $a_\gamma$ . The Sudakov factor  $S_\Gamma$  requires the knowledge of the three-loop coefficients  $\beta_2$  and  $\Gamma_2$  and reads with  $r = \alpha_s(\mu)/\alpha_s(\nu)$

$$\begin{aligned} S_\Gamma(\nu, \mu) &= \frac{\Gamma_0}{4\beta_0^2} \left\{ \frac{4\pi}{\alpha_s(\nu)} \left( 1 - \frac{1}{r} - \ln r \right) + \left( \frac{\Gamma_1}{\Gamma_0} - \frac{\beta_1}{\beta_0} \right) (1 - r + \ln r) + \frac{\beta_1}{2\beta_0} \ln^2 r \right. \\ &\quad + \frac{\alpha_s(\nu)}{4\pi} \left[ \left( \frac{\beta_1 \Gamma_1}{\beta_0 \Gamma_0} - \frac{\beta_2}{\beta_0} \right) (1 - r + r \ln r) + \left( \frac{\beta_1^2}{\beta_0^2} - \frac{\beta_2}{\beta_0} \right) (1 - r) \ln r \right. \\ &\quad \left. \left. - \left( \frac{\beta_1^2}{\beta_0^2} - \frac{\beta_2}{\beta_0} - \frac{\beta_1 \Gamma_1}{\beta_0 \Gamma_0} + \frac{\Gamma_2}{\Gamma_0} \right) \frac{(1 - r)^2}{2} \right] + \dots \right\}. \end{aligned} \quad (80)$$

The next-to-leading-logarithmic Sudakov factor  $U(\mu_h, \mu_i)$  can be obtained by combining the above expressions according to (76) and expanding out terms of order  $\alpha_s$ .

## B Partially integrated decay rates

With the exception of the combined cut on the lepton energy  $E_l$  and the hadronic quantity  $s_H^{\text{max}}$  studied in Section 5.5, all other partial rates investigated in our analysis can be derived by first integrating the triple differential decay rate (23) over the lepton energy  $E_l \geq E_0$  and  $P_- \leq P_-^{\text{max}}$  analytically, where the quantity  $P_-^{\text{max}}$  (and in principle even  $E_0$ ) may depend on the value of  $P_+$ . The remaining integration over  $P_+$  is then performed numerically. In such a situation, we need to evaluate the partially integrated decay rate

$$\frac{d\Gamma_u}{dP_+} = \int_{P_+}^{P_-^{\text{max}}} dP_- \int_{P_+}^{\min(P_-, M_B - 2E_0)} dP_l \frac{d^3\Gamma_u}{dP_l dP_- dP_+}. \quad (81)$$

Changing variables from  $P_-$  to  $y$  defined in (25), the constraint  $P_- \leq P_-^{\max}$  translates into the integration domain  $0 \leq y \leq y_{\max}$ , where in analogy to (25) we define

$$y_{\max} = \frac{P_-^{\max} - P_+}{M_B - P_+}, \quad y_0 = \frac{P_l^{\max} - P_+}{M_B - P_+} = 1 - \frac{2E_0}{M_B - P_+}. \quad (82)$$

From the phase-space relation (2) it follows that a cut on the lepton energy has no effect if  $y_0 \geq y_{\max}$ . In general, we can state the result as

$$\frac{d\Gamma(y_{\max}, y_0)}{dP_+} = \begin{cases} \Gamma_u^A(y_{\max}) & ; \quad y_{\max} \leq y_0, \\ \Gamma_u^A(y_0) + \Gamma_u^B(y_{\max}, y_0) - \Gamma_u^B(y_0, y_0) & ; \quad y_{\max} > y_0, \end{cases} \quad (83)$$

where we distinguish between type- $A$ , which is independent on  $y_0$ , and type- $B$ , which carries all the  $y_0$  dependence. Explicitly, we obtain

$$\begin{aligned} \Gamma_u^A(y_{\max}) &= \frac{G_F^2 |V_{ub}|^2}{96\pi^3} (M_B - P_+)^5 U(\mu_h, \mu_i) \int_0^{y_{\max}} dy y^{2-2a_\Gamma} [(3-2y) \mathcal{F}_1 + 6(1-y) \mathcal{F}_2 + y \mathcal{F}_3], \\ \Gamma_u^B(y_{\max}) &= \frac{G_F^2 |V_{ub}|^2}{96\pi^3} (M_B - P_+)^5 U(\mu_h, \mu_i) \int_{y_0}^{y_{\max}} dy y^{-2a_\Gamma} y_0 \\ &\quad \times [(6y(1+y_0) - 6y^2 - y_0(3+2y_0)) \mathcal{F}_1 + 6y(1-y) \mathcal{F}_2 + y_0(3y-2y_0) \mathcal{F}_3]. \end{aligned} \quad (84)$$

When the kinematical power corrections in (30) are Taylor expanded as in (32) and (33), the resulting integrals over  $y$  can be expressed in terms of the master functions  $I_n(b, z)$  given in eq. (86) of [9]. The resulting expressions are used to obtain the numbers in the various tables in Section 5.

We now list the values of  $y_0$  and  $y_{\max}$  for the different cuts studied in Section 5. Whenever a cut  $E_l \geq E_0$  on the charged-lepton energy is applied, we have

$$y_0 = 1 - \frac{2E_0}{M_B - P_+}. \quad (85)$$

For an additional cut  $P_+ \leq \Delta_P$ , we have  $y_{\max} = 1$  and  $0 \leq P_+ \leq \min(\Delta_P, M_B - 2E_0)$ . For a cut on hadronic invariant mass,  $M_X \leq M_0$ , we have

$$y_{\max} = \frac{\min(M_B, M_0^2/P_+) - P_+}{M_B - P_+} \quad (86)$$

and  $0 \leq P_+ \leq \min(M_0, M_B - 2E_0)$ . For a cut on leptonic invariant mass,  $q^2 \geq q_0^2$ , we have

$$y_{\max} = 1 - \frac{q_0^2}{(M_B - P_+)^2} \quad (87)$$

and  $0 \leq P_+ \leq \min(M_B - q_0, M_B - 2E_0)$ . Finally, for the combined  $M_X - q^2$  cut we take the minimum of the previous two  $y_{\max}$  values.

## References

- [1] B. Aubert *et al.* [BaBar Collaboration], Phys. Rev. Lett. **94**, 161803 (2005) [hep-ex/0408127].
- [2] K. Abe *et al.* [Belle Collaboration], Phys. Rev. D **71**, 072003 (2005) [Erratum-ibid. D **71**, 079903 (2005)] [hep-ex/0408111].
- [3] M. Neubert, Phys. Rev. D **49**, 3392 (1994) [hep-ph/9311325].
- [4] M. Neubert, Phys. Rev. D **49**, 4623 (1994) [hep-ph/9312311].
- [5] I. I. Y. Bigi, M. A. Shifman, N. G. Uraltsev and A. I. Vainshtein, Int. J. Mod. Phys. A **9**, 2467 (1994) [hep-ph/9312359].
- [6] G. P. Korchemsky and G. Sterman, Phys. Lett. B **340**, 96 (1994) [hep-ph/9407344].
- [7] R. Akhoury and I. Z. Rothstein, Phys. Rev. D **54**, 2349 (1996) [hep-ph/9512303].
- [8] C. W. Bauer and A. V. Manohar, Phys. Rev. D **70**, 034024 (2004) [hep-ph/0312109].
- [9] S. W. Bosch, B. O. Lange, M. Neubert and G. Paz, Nucl. Phys. B **699**, 335 (2004) [hep-ph/0402094].
- [10] E. Gardi, JHEP **0404**, 049 (2004) [hep-ph/0403249].
- [11] M. Neubert, Eur. Phys. J. C **40**, 165 (2005) [hep-ph/0408179].
- [12] B. Blok, L. Koyrakh, M. A. Shifman and A. I. Vainshtein, Phys. Rev. D **49**, 3356 (1994) [Erratum-ibid. D **50**, 3572 (1994)] [hep-ph/9307247].
- [13] A. V. Manohar and M. B. Wise, Phys. Rev. D **49**, 1310 (1994) [hep-ph/9308246].
- [14] S. W. Bosch, B. O. Lange, M. Neubert and G. Paz, Phys. Rev. Lett. **93**, 221801 (2004) [hep-ph/0403223].
- [15] F. J. Tackmann, hep-ph/0503095.
- [16] S. W. Bosch, M. Neubert and G. Paz, JHEP **0411**, 073 (2004) [hep-ph/0409115].
- [17] A. K. Leibovich, I. Low and I. Z. Rothstein, Phys. Rev. D **61**, 053006 (2000) [hep-ph/9909404].
- [18] A. K. Leibovich, I. Low and I. Z. Rothstein, Phys. Lett. B **486**, 86 (2000) [hep-ph/0005124].
- [19] M. Neubert, Phys. Lett. B **513**, 88 (2001) [hep-ph/0104280].
- [20] K. G. Chetyrkin, M. Misiak and M. Munz, Phys. Lett. B **400**, 206 (1997) [Erratum-ibid. B **425**, 414 (1998)] [hep-ph/9612313].

- [21] F. De Fazio and M. Neubert, JHEP **9906**, 017 (1999) [hep-ph/9905351].
- [22] C. Greub, T. Hurth and D. Wyler, Phys. Rev. D **54**, 3350 (1996) [hep-ph/9603404].
- [23] A. Ali and C. Greub, Phys. Lett. B **361**, 146 (1995) [hep-ph/9506374].
- [24] A. L. Kagan and M. Neubert, Eur. Phys. J. C **7**, 5 (1999) [hep-ph/9805303].
- [25] R. J. Hill, T. Becher, S. J. Lee and M. Neubert, JHEP **0407**, 081 (2004) [hep-ph/0404217].
- [26] T. Becher, R. J. Hill, B. O. Lange and M. Neubert, Phys. Rev. D **69**, 034013 (2004) [hep-ph/0309227].
- [27] C. W. Bauer, M. E. Luke and T. Mannel, Phys. Rev. D **68**, 094001 (2003) [hep-ph/0102089].
- [28] C. W. Bauer, M. Luke and T. Mannel, Phys. Lett. B **543**, 261 (2002) [hep-ph/0205150].
- [29] A. K. Leibovich, Z. Ligeti and M. B. Wise, Phys. Lett. B **539**, 242 (2002) [hep-ph/0205148].
- [30] M. Neubert, Phys. Lett. B **543**, 269 (2002) [hep-ph/0207002].
- [31] K. S. M. Lee and I. W. Stewart, hep-ph/0409045.
- [32] M. Beneke, F. Campanario, T. Mannel and B. D. Pecjak, hep-ph/0411395.
- [33] A. F. Falk and M. Neubert, Phys. Rev. D **47**, 2965 (1993) [hep-ph/9209268].
- [34] M. Neubert, Phys. Rept. **245**, 259 (1994) [hep-ph/9306320].
- [35] G. Martinelli, M. Neubert and C. T. Sachrajda, Nucl. Phys. B **461**, 238 (1996) [hep-ph/9504217].
- [36] M. Neubert, Phys. Lett. B **393**, 110 (1997) [hep-ph/9610471].
- [37] A. F. Falk, M. E. Luke and M. J. Savage, Phys. Rev. D **49**, 3367 (1994) [hep-ph/9308288].
- [38] M. Neubert, JHEP **0007**, 022 (2000) [hep-ph/0006068].
- [39] M. Neubert and T. Becher, Phys. Lett. B **535**, 127 (2002) [hep-ph/0105217].
- [40] N. Uraltsev, Int. J. Mod. Phys. A **14**, 4641 (1999) [hep-ph/9905520].
- [41] I. I. Y. Bigi and N. G. Uraltsev, Nucl. Phys. B **423**, 33 (1994) [hep-ph/9310285].
- [42] M. Neubert and C. T. Sachrajda, Nucl. Phys. B **483**, 339 (1997) [hep-ph/9603202].
- [43] M. B. Voloshin, Phys. Lett. B **515**, 74 (2001) [hep-ph/0106040].
- [44] T. O. Meyer, “Limits on weak annihilation in inclusive charmless semileptonic  $B$  decays”, PhD Thesis, Cornell University, (2005).

- [45] M. Neubert, hep-ph/0411027.
- [46] B. Aubert *et al.* [BaBar Collaboration], Phys. Rev. Lett. **93**, 011803 (2004) [hep-ex/0404017].
- [47] M. Beneke, Phys. Lett. B **434**, 115 (1998) [hep-ph/9804241].
- [48] A. H. Hoang, Z. Ligeti and A. V. Manohar, Phys. Rev. D **59**, 074017 (1999) [hep-ph/9811239].
- [49] I. I. Y. Bigi, M. A. Shifman, N. Uraltsev and A. I. Vainshtein, Phys. Rev. D **56**, 4017 (1997) [hep-ph/9704245].
- [50] M. Neubert, Phys. Lett. B **612**, 13 (2005) [hep-ph/0412241].
- [51] T. van Ritbergen, Phys. Lett. B **454**, 353 (1999) [hep-ph/9903226].
- [52] A. F. Falk, Z. Ligeti and M. B. Wise, Phys. Lett. B **406**, 225 (1997) [hep-ph/9705235].
- [53] I. I. Y. Bigi, R. D. Dikeman and N. Uraltsev, Eur. Phys. J. C **4**, 453 (1998) [hep-ph/9706520].
- [54] C. W. Bauer, Z. Ligeti and M. E. Luke, Phys. Lett. B **479**, 395 (2000) [hep-ph/0002161].
- [55] C. W. Bauer, Z. Ligeti and M. E. Luke, Phys. Rev. D **64**, 113004 (2001) [hep-ph/0107074].
- [56] B. Aubert *et al.* [BaBar Collaboration], hep-ex/0408045.
- [57] O. V. Tarasov, A. A. Vladimirov and A. Y. Zharkov, Phys. Lett. B **93**, 429 (1980).
- [58] S. Moch, J. A. M. Vermaseren and A. Vogt, Nucl. Phys. B **688**, 101 (2004) [hep-ph/0403192].